Chromosomes and Gene Expression
Microbiology and Infectious Disease

PI(3,4,5)P3 allosteric regulation of repressor activator protein 1 controls antigenic variation in trypanosomes

Abdoulie O. Touray, Rishi Rajesh, Tony Isebe, Tamara Sternlieb, Mira Loock, Oksana Kutova, Igor Cestari

Institute of Parasitology, McGill University, Sainte-Anne-de-Bellevue, QC H9X 3V9, Canada • Division of Experimental Medicine, Department of Medicine, McGill University, Montreal, QC, H4A 3J1, Canada

Reviewed Preprint

Revised by authors after peer review.

About eLife's process

Reviewed preprint version 3
November 7, 2023

Reviewed preprint version 2
August 31, 2023 (this version)

Reviewed preprint version 1
July 12, 2023

Sent for peer review
May 17, 2023

Posted to preprint server
May 11, 2023

Abstract

African trypanosomes evade host immune clearance by antigenic variation, causing persistent infections in humans and animals. These parasites express a homogeneous surface coat of variant surface glycoproteins (VSGs). They transcribe one out of hundreds of VSG genes at a time from telomeric expression sites (ESs) and periodically change the VSG expressed by transcriptional switching or recombination. The mechanisms underlying the control of VSG switching and its developmental silencing remain elusive. We report that telomeric ES activation and silencing entail an on/off genetic switch controlled by a nuclear phosphoinositide signaling system. This system includes a nuclear phosphatidylinositol 5-phosphatase (PIP5Pase), its substrate PI(3,4,5)P3, and the repressor-activator protein 1 (RAP1). RAP1 binds to ES sequences flanking VSG genes via its DNA binding domains and represses VSG transcription. In contrast, PI(3,4,5)P3 binds to the N-terminus of RAP1 and controls its DNA binding activity. Transient inactivation of PIP5Pase results in the accumulation of nuclear PI(3,4,5)P3, which binds RAP1 and displaces it from ESs, activating transcription of silent ESs and VSG switching. The system is also required for the developmental silencing of VSG genes. The data provides a mechanism controlling reversible telomere silencing essential for the periodic switching in VSG expression and its developmental regulation.

eLife assessment

Trypanosoma brucei evades mammalian humoral immunity through the expression of different variant surface glycoprotein genes. In this **fundamental** paper, the authors extend previous observations that TbRAP1 both interacts with PIP5Pase and binds PI(3,4,5)P3, indicating a role for PI(3,4,5)P3 binding and suggesting that antigen switching is signal dependent. While much of the evidence is **compelling**, the work would benefit from further controls to rule out that any of the observed effects come from the protein tags used.

Introduction

Antigenic variation is a strategy of immune evasion used by many pathogens to maintain persistent infections and entails changes in surface antigens to escape host immune clearance. The single-celled protozoa *Trypanosoma brucei spp.* circulate in the mammalian host bloodstream and periodically change their variant surface glycoprotein (VSG) coat to evade antibody clearance by antigenic variation (1). *T. brucei* have over 2,500 VSG genes and pseudogenes, primarily on subtelomeres, and ~20 telomeric expression sites (ESs), each containing a VSG gene (**Fig 1A**). Only one VSG gene is transcribed at a time from a telomeric ES. Antigenic variation occurs via transcriptional switching between ESs or VSG gene recombination within ESs (1). The active VSG gene is developmentally regulated, and its expression is silenced in parasites encountered in the tsetse fly vector, e.g., procyclic and epimastigote forms. Epimastigotes develop into transmissible metacyclic trypomastigotes, which re-activate VSG gene expression before infecting mammals. The coordinated activation and silencing of telomeric ESs is essential for the periodic switch in VSG gene expression during antigenic variation and VSG developmental regulation; however, the mechanisms underlying the control of this process remain unknown.

The expressed VSG gene is transcribed by RNA polymerase I (RNAP I) from a compartment outside the nucleolus termed ES body (ESB) (2). Transcription initiates in all ESs but only elongates through one ES (hereafter called active ES), resulting in VSG monogenic expression. The silencing of ES VSG genes involves its proximity to telomeres (3, 4) and the telomere-associated factor repressor activator protein 1 (RAP1) (5). RAP1 is conserved among eukaryotes (5–8) and functions in telomere silencing (5, 8), telomere end protection (9–11), and non-telomeric gene regulation in mammals and yeast (8, 11). Histones and chromatin-modifying enzymes, such as histone methyltransferase and bromodomain proteins, also associate with ESs and contribute to their repression (12–15). In contrast, the active ES is depleted of nucleosomes (12) and enriched in proteins that facilitate its transcription, e.g., VSG exclusion (VEX) 1 and 2 and ES body 1 (ESB1), and processing of the highly abundant VSG mRNAs (16, 17).

The mechanisms underlying the initiation or control of VSG switching remain unknown. Antigenic variation was thought to occur stochastically (18) with the DNA break and repair machinery involved in VSG recombination (19–22). However, we showed that phosphoinositide signaling plays a role in the expression and switching of VSG genes (23, 24). This system entails the plasma membrane/cytosolic-localized phosphatidylinositol phosphate 5-kinase (PIP5K) and phospholipase C (PLC) (23), and the nuclear phosphatidylinositol phosphate 5-phosphatase (PIP5Pase). The PIP5Pase enzyme interacts with RAP1 (24, 25), and either protein knockdown results in the transcription of all ESs simultaneously (5, 23, 24). RAP1 and PIP5Pase interact with other nuclear proteins, including nuclear lamina, nucleic acid binding proteins, and protein kinases and phosphatases (24). The involvement of phosphoinositide signaling in VSG expression and switching implied that signaling and regulatory processes have a role in antigenic variation linking cytosolic and nuclear proteins to control transcriptional and recombination mechanisms.

We report here that PIP5Pase, its substrate PI(3,4,5)P3, and its binding partner RAP1 form a genetic regulatory circuit that controls ES activation and repression. We show that RAP1 binds to silent telomeric ESs sequences flanking the VSG genes, and the binding is essential for VSG transcriptional repression. This association is regulated by PI(3,4,5)P3, which binds to the N-terminus of RAP1, acting as an allosteric regulator controlling RAP1-ES interactions. The system depends on PIP5Pase catalytic activity, which dephosphorylates PI(3,4,5)P3 and prevents its binding to RAP1. Inactivation of PIP5Pase results in PI(3,4,5)P3 and RAP1 binding, which displaces RAP1 from ESs, leading to transcription and switching of VSGs in the population. Hence, PIP5Pase activity is required for RAP1 association with silent ESs and VSG gene transcriptional control. The

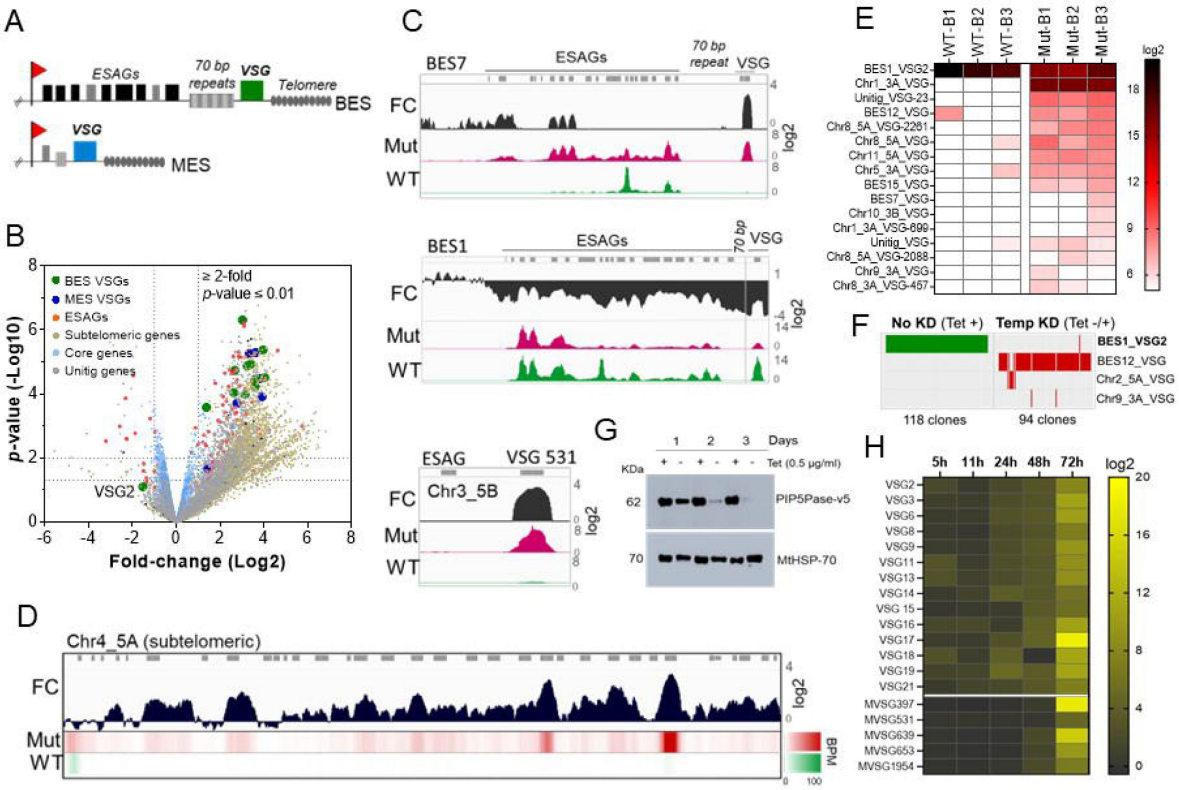

Fig 1.

PIP5Pase activity is essential for VSG gene silencing and switching.

A) Diagram of bloodstream-form ESs (BES, top) and metacyclic-form ESs (MES, bottom). B) RNA-seq analysis of *T. brucei* bloodstream forms comparing 24h exclusive expression of Mut to WT PIP5Pase. FC, fold-change. Horizontal dotted lines indicate *p*-values at 0.05 and 0.01. Vertical dotted lines, FC at 2-fold. Unitig genes, genes not assembled in the reference genome. C-D) RNA-seq read coverage and FC (Mut vs WT) of silent BES7 (C, top), the active BES1 (C, middle), a silent MES (C, bottom), and chromosome 4 subtelomere (D). Heat-map in D shows RNA-seq bins per million (BPM) reads. Gray rectangles represent genes. A 99.9% reads mapping probability to the genome (mapQ>30) retained alignments to subtelomeric regions. E) VSG-seq analysis of *T. brucei* bloodstream forms after temporary (24h) exclusive expression of Mut PIP5Pase, and re-expression for 60h of WT PIP5Pase. B1-B3, biological replicates. The color shows normalized read counts per million. A 3'-end conserved VSG sequence was used to capture VSG mRNAs (41). See Table S1 for data and gene IDs of VSGs. F) VSG-seq from isolated clones after PIP5Pase temporary knockdown (24h) followed by its re-expression (Tet - /+) and cloning for 5-7 days. Clones of non-knockdown (tet +) cells were analyzed as controls. BES1_VSG2 (Tb427_000016000), BES12_VSG (Tb427_000008000), Chr2_5A_VSG (Tb427_000284800), Chr9_3A_VSG (Tb427_000553800). G) Western blot of V5-tagged PIP5Pase knockdown in *T. brucei* procyclic forms. The membrane was stripped and reprobed with anti-mitochondrial heat shock protein 70 (MtHSP70). H) Expression analysis of ES VSG genes after knockdown of PIP5Pase in procyclic forms by real-time PCR. Data are the result of three biological replicates.

regulatory system is essential for VSG developmental silencing, and temporal disruption of this nuclear signaling system results in VSG switching. The data indicate a molecular mechanism by which ESs are periodically turned on and off during antigenic variation and parasite development.

Results

PIP5Pase activity controls VSG switching and developmental silencing

To investigate the role of PIP5Pase activity in VSG gene expression and switching, we performed gene expression analysis in *T. brucei* bloodstream forms that exclusively express a wildtype (WT) or a catalytic mutant D360A/N362A (Mut) PIP5Pase; the latter is unable to dephosphorylate PI(3,4,5)P3 (24). The exclusive expression cells have the endogenous PIP5Pase alleles replaced by drug-selectable markers, a tetracycline (tet)-regulatable PIP5Pase allele introduced in the silent rDNA spacer, and a V5-tagged WT or Mut PIP5Pase allele in the constitutively expressed tubulin loci (24). In the absence of tet, the cells exclusively express the WT or Mut PIP5Pase allele (24). We performed RNA-seq after 24h exclusive expression of the WT or Mut PIP5Pase with Oxford nanopore sequencing (~500 bp reads) to distinguish the VSG genes expressed. The expression of the Mut PIP5Pase resulted in 1,807 genes upregulated and 33 downregulated (**Fig 1B**, ≥ 2-fold change, *p*-value ≤ 0.01, Data S1). Notably, all silent ES VSG genes were upregulated (**Fig 1B** and **C**), consistent with their transcription. In contrast, there was a ~10-fold decrease in the active VSG (VSG2) and ESAG mRNAs (**Fig 1B** and **C**), implying decreased expression of the active ES (BES1) genes, perhaps resulting from competition among ESs for polymerase or factors required for their transcription. The remaining upregulated genes were primarily from silent subtelomeric arrays, largely VSG genes and pseudogenes (**Fig 1B** and **D**), indicating that PIP5Pase activity is also required for subtelomeric ES repression. Other upregulated genes included primarily retrotransposons, endonucleases, and RNA polymerases, but most chromosome core genes (Pol II and Pol III transcribed genes) were not significantly affected (**Fig 1B**). Re-establishing expression of WT PIP5Pase for 60h after its 24h withdrawal restored VSG monogenic expression. However, analysis of this population by VSG-seq revealed the expression of several VSGs other than the initially expressed VSG2 indicating a switch in VSG expression (**Fig 1E**). In contrast, only a few VSGs were detected in cells expressing WT PIP5Pase by VSG-seq (**Fig 1E**). To verify PIP5Pase role in VSG switching, we knocked down PIP5Pase for 24h (Tet -), then restored its expression (Tet +) and isolated clones by limit dilution and growth for 5-7 days (Fig S1). Analysis of isolated clones after temporary PIP5Pase knockdown (Tet -/+) confirmed VSG switching in 93 out of 94 (99%) analyzed clones (**Fig 1F**, Fig S1). The cells switched to express VSGs from silent ESs or subtelomeric regions, indicating switching by transcription or recombination mechanisms. Moreover, no switching was detected in 118 isolated clones from cells continuously expressing WT PIP5Pase (Tet +, **Fig 1F**). The data imply that PIP5Pase activity can control the transcription and switching of VSGs.

The active VSG gene is expressed in bloodstream forms but silenced during parasite development to the insect stage procyclic forms. To determine whether PIP5Pase is required for VSG developmental silencing, we generated procyclic conditional null cells expressing a tet-regulatable V5-tagged PIP5Pase (Fig S2). Immunofluorescence analysis showed that PIP5Pase-V5 localizes in the nucleus of procyclic forms (Fig S2), as in bloodstream forms (23). Western analysis showed that PIP5Pase-V5 proteins were eliminated 72h after knockdown (**Fig 1G**), and growth arrest was detected after five days of knockdown (Fig S2). Gene expression analysis showed a 5-15 log2-fold upregulation of all ES VSG genes at 72h (**Fig 1H**) at a time when cells are viable and dividing. The data indicate that VSG switching and developmental silencing depend on PIP5Pase activity.

RAP1 bind to sequences flanking VSG genes in silent telomeric ESs

Because PIP5Pase and its substrate PI(3,4,5)P3 interact with RAP1 (24), we postulated that VSG silencing might involve the regulation of RAP1's repressive function. We showed that RAP1 binds telomeric or 70 bp repeats (24), but it is unknown if it binds to other ES sequences or genomic loci. We performed ChIP-seq with a cell line expressing an *in-situ* HA-tagged RAP1 and nanopore sequencing (~500 bp reads). We found that RAP1-HA binds primarily to silent ESs at the 70 bp and telomeric repeats, which are sequences upstream and downstream of the VSG genes in bloodstream-form ESs, respectively (**Fig 2A-B, E** and Fig S3; *p*-values < 10^{-4}). There was also a slight enrichment of RAP1-HA in the 50 bp repeat sequences preceding the ES promoters (**Fig 2A** and Fig S3; *p*-values < 10^{-4}). However, RAP1-HA did not bind significantly to genes, including VSG genes or pseudogenes in the ESs or subtelomeric regions (**Fig 2A-B, F**). Notably, analysis of uniquely mapped reads showed that RAP1-HA was depleted from the active ES (**Fig 2C-D** and Fig S4), consistent with RAP1 having a repressive function. The RAP1-HA bound sequences are rich in TAAs and GTs, including the 70 bp $(TTA)_7(GT/A)_9$ and telomeric $(TTAGGG)_n$ repeats (**Fig 2A**), but also T and G/T rich sequences downstream of VSG genes. RAP1-HA was also bound to metacyclic ESs at AT/GC-rich or (TAACCC)n repeat sequences near VSG genes (**Fig 2E**, *p*-values < 10^{-4}, Fig S5). RAP1-HA also bound sparsely to subtelomeric regions, including centromeres (**Fig 2F**, *p*-values < 10^{-4}), which are AT-rich in trypanosomes (26), and some binding sites overlapped with the centromeric protein kinetoplastid kinetochore 2 (KKT2) (27). Other poorly enriched RAP1-HA peaks in the subtelomeric regions reflect residual ES sequences from recombination (**Fig 2F**). Hence, RAP1-HA binds primarily to telomeric and 70 bp repeats within silent ESs. The 70 bp repeats are ES-specific sites for RAP1 binding near silent VSG genes.

To confirm RAP1 binding to ES sequences, we expressed and purified from *E. coli* recombinant 6xHis-tagged *T. brucei* RAP1 (rRAP1) (**Fig 3A-B**). We performed electrophoretic mobility shift assays (EMSA) using rRAP1 and biotinylated telomeric repeats, 70 bp repeat, or a scrambled telomeric repeat sequence as a control. rRAP1 bound to telomeric and 70 bp repeats but not to the scrambled DNA sequence (**Fig 3C**). We obtained similar results by microscale thermophoresis (MST) kinetics using rRAP1 and Cy5-labelled DNA sequences (**Fig 3D**, Fig S6). The MST analysis revealed a Kd of 24.1 and 10 nM of rRAP1 for telomeric and 70 bp repeats, respectively (**Table 1**). RAP1 has two DNA binding domains, a central Myb (position E426-Q500) and a C-terminal Myb-like (MybL, position E639-R761) domain (**Fig 3A**), and a divergent BRCT domain (S198-P385) (5), which is involved in RAP1 self-interaction (28) and perhaps other protein interactions (23, 24). To identify which RAP1 domain mediates DNA interactions, we performed EMSA with $rRAP1^{1\text{-}300}$ (aa positions in superscript), $rRAP1^{301\text{-}560}$, and $rRAP1^{561\text{-}855}$, the last two fragments encompass the Myb and MybL domains, respectively (**Fig 3A-B**). Both $rRAP1^{301\text{-}560}$ and $rRAP1^{561\text{-}855}$ proteins bound to telomeric or 70 bp repeats (**Fig 3E-F**, Fig S6), but no DNA binding was detected with the N-terminal $rRAP1^{1\text{-}300}$ (**Fig 3G**). Because all proteins were His-tagged and no binding was detected to scrambled DNA nor with $rRAP1^{1\text{-}300}$ (also His-tagged), unspecific DNA binding by the His-tag is ruled out. Notably, disruption of the MybL domain sequence did not eliminate RAP1-telomere binding *in vivo* (29). Concurring, our data imply that the Myb domain can compensate for the MybL disruption and show that both Myb and MybL can independently and directly bind to 70 bp and telomeric repeats.

PIP5Pase activity controls PI(3,4,5)P3 binding to the N-terminus of RAP1

We found in the N-terminus of RAP1 a villin headpiece (VHP) domain (**Fig 3A**, position Y59 to F94, *e*- value < 10^{-4}), which is typically present in Villin proteins and binds phosphoinositides (30). *T. brucei* RAP1 VHP domain is conserved (~27% aa identity) with other VHPs in Villin proteins forming a three helices fold over a hydrophobic core (31, 32) (**Fig 4A**), which is essential for phosphoinositide binding (30). We performed binding assays with rRAP1 and biotinylated phosphoinositides (25) and confirmed that rRAP1 binds specifically to PI(3,4,5)P3

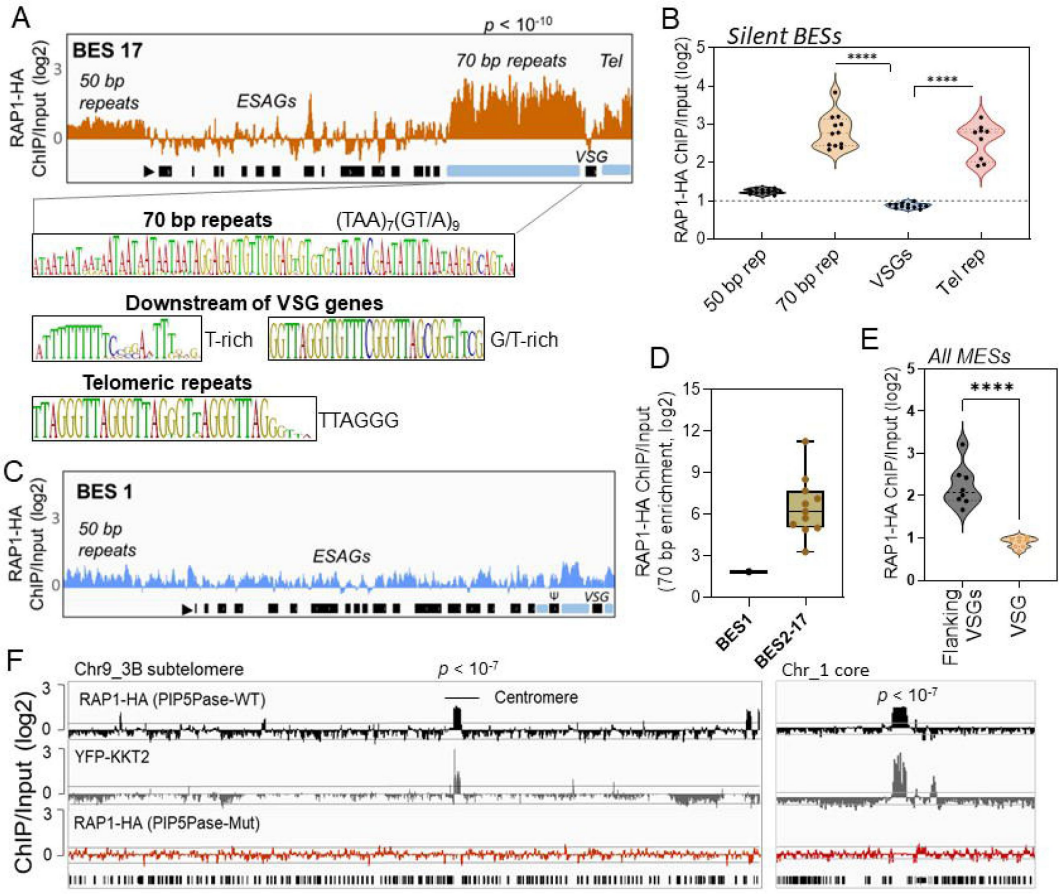

Fig 2.

ChIP-seq analysis of RAP1-HA in *T. brucei.*

A) RAP1-HA binding sites on the silent BES17. Data show fold-change comparing ChIP vs Input. Below is the sequence bias of RAP1-HA bound regions. Black rectangles, ES genes; black triangle, ES promoter; cyan rectangle, 70 bp and telomeric repeats. B) RAP1-HA binding to selected regions in silent BES sequences. Each dot represents the mean of a silent BES. C) RAP1-HA enrichment to the active BES1 (fold-change comparing ChIP vs Input). See Fig S4 for additional read mapping and filtering analysis. D) Comparison of RAP1-HA binding to 70 bp in silent and active ESs. E) RAP1-HA enrichment over all MESs. Flanking VSGs, DNA sequences upstream or downstream of VSG genes in MESs. F) RAP1-HA binding to subtelomere 3B of chromosome (Chr) 9 (left) or chromosome 1 core (right). Yellow fluorescent protein (YFP)-tagged KKT2 protein ChIP-seq from (27) is shown. RAP1-HA ChIP-seq in cells expressing Mut PIP5Pase is shown below. *p*-values (*p)* were calculated using Model-based Analysis of ChIP-Seq (MACS) from three biological replicates. Data show fold-change of ChIP vs Input analysis. See Table S2 and Data S2 for detailed statistics. ****, *p*-value < 0.0001.

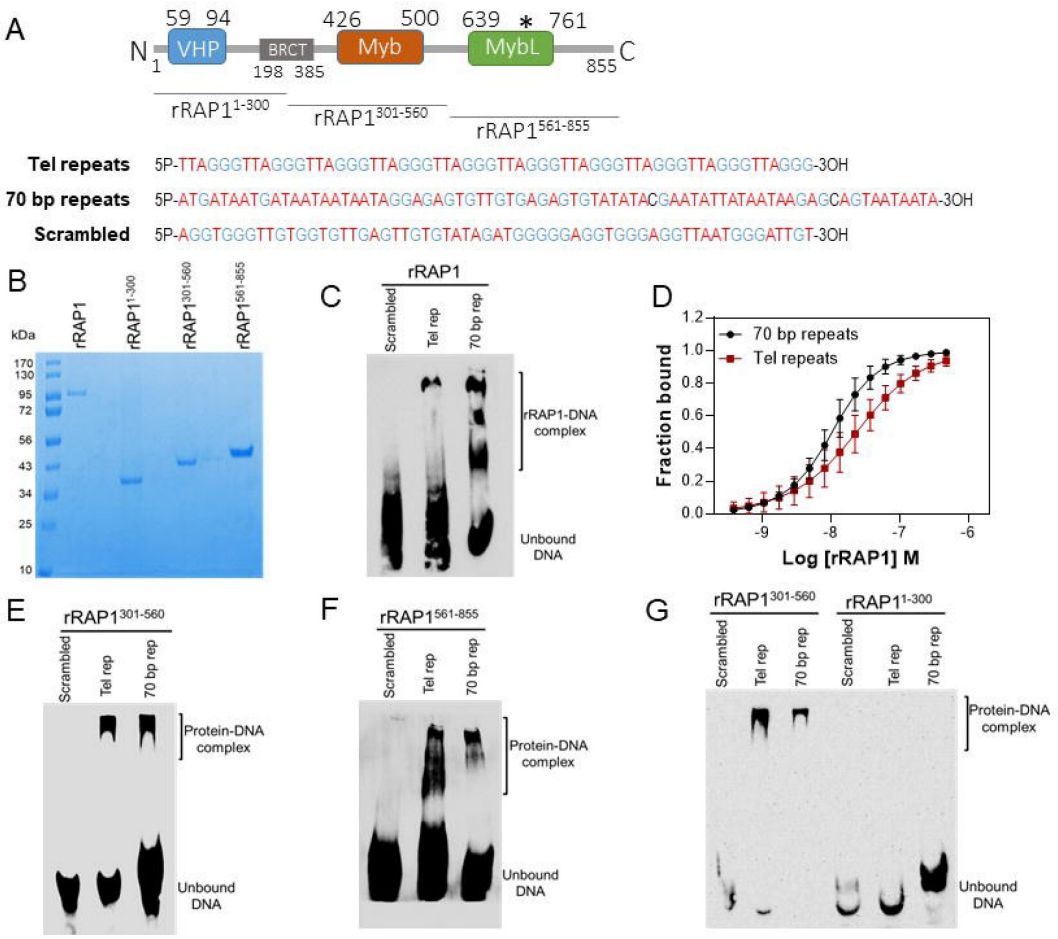

Fig 3.

rRAP1 binds to telomeric and 70 bp repeats via its Myb and MybL domain.

A) Top, RAP1 diagram shows VHP, BRCT, Myb and MybL domains. Numbers indicate residue positions; asterisk, nuclear targeting sequence. Bottom, telomeric (10 repeats), 70 bp (one repeat), or scrambled (generated from telomeric repeats) sequences used in binding assays. B) His-tagged rRAP1, rRAP1$^{1-300}$, rRAP$^{301-560}$, and rRAP1$^{561-855}$ resolved in 10% SDS/PAGE and Coomassie-stained. C) EMSA of His-tagged rRAP1 with biotinylated telomeric repeats (Tel rep), 70 repeats (70 bp rep), or scrambled sequences resolved in 6% native/PAGE and developed with Streptavidin-HRP. D) MST binding kinetics of rRAP1 with Cy5-labelled telomeric repeats or 70 bp repeats. Data shown are the mean ± SDM of four biological replicates. E-G) EMSA of rRAP1$^{301-560}$ (E), rRAP1$^{561-855}$ (F), or rRAP1$^{1-300}$ (G) with telomeric, 70 bp repeats, or scrambled sequences resolved in 6% native/PAGE. rRAP1$^{301-560}$ were used as a positive control in G.

Interactions	Kd [M] ± SDM
rRAP1 + Telomeric repeats	$24.1x10^{-9} \pm 2.0x10^{-9}$
rRAP1 + 70 bp repeats	$10.0x10^{-9} \pm 0.33x10^{-9}$
rRAP1 + PI(3,4,5)P3	$19.7x10^{-6} \pm 2.8x10^{-6}$
rRAP1 + PI(4,5)P2	No binding
rRAP1 + Telomeric repeats + PI(3,4,5)P3	$154.6x10^{-9} \pm 14.2\ x10^{-9}$
rRAP1 + Telomeric repeats + PI(4,5)P2	$19.4x10^{-9} \pm 1.5\ x10^{-9}$
rRAP1 + 70 bp repeats + PI(3,4,5)P3	$187.7x10^{-9} \pm 29.9x10^{-9}$
rRAP1 + 70 bp repeats + PI(4,5)P2	$17.5x10^{-8} \pm 0.9\ x10^{-9}$

Table 1.

Binding kinetics of rRAP1 to telomeric repeats, 70 bp repeats, and phosphoinositides. Data show the mean ± standard deviation of the mean (SDM).

(Fig S6) (24). Moreover, we found that rRAP1$^{1-300}$ binds to PI(3,4,5)P3 (**Fig 4B**), but not other phosphoinositides or inositol phosphates tested (**Fig 4C**) and the binding was competed by a molar excess of unlabelled PI(3,4,5)P3 (**Fig 4D**). However, no PI(3,4,5)P3 binding was detected with rRAP1$^{301-560}$ or rRAP1$^{561-855}$ proteins, indicating that RAP1 binds to PI(3,4,5)P3 via its N-terminus containing the VHP domain. Moreover, binding kinetics by differential scanning fluorescence with unlabelled phosphoinositides showed that rRAP1 binds to PI(3,4,5)P3 with a Kd of 19.7 μM (**Fig 4E**, **Table 1**). To determine if RAP1 binds to PI(3,4,5)P3 *in vivo,* we *in-situ* HA-tagged RAP1 in cells that express the WT or Mut PIP5Pase and analyzed endogenous PI(3,4,5)P3 levels associated with immunoprecipitated RAP1-HA. There were ~100-fold more PI(3,4,5)P3 associated with RAP1-HA in cells expressing the Mut than the WT PIP5Pase (**Fig 4F**, Fig S7). In contrast, there was a mild but not significant difference in the total cellular PI(3,4,5)P3 levels comparing cells expressing WT versus Mut PIP5Pase (**Fig 4F**), implying that PIP5Pase activity controls a localized pool of PI(3,4,5)P3 in the nucleus available for RAP1 binding. Hence, RAP1 binds specifically to PI(3,4,5)P3 via its N-terminus in a PIP5Pase activity-dependent fashion.

PI(3,4,5)P3 is an allosteric regulator of RAP1 and controls telomeric ES repression

Because RAP1 binds to PI(3,4,5)P3 via its N-terminus and to ESs via its central and C-terminus Myb and Myb-L domains, we posited that PI(3,4,5)P3 binds to RAP1 and controls its association with ESs. We performed EMSA binding assays and found that PI(3,4,5)P3 inhibited rRAP1 binding to telomeric repeats in a dose-dependent fashion, but no inhibition was detected with PI(4,5)P2 (**Fig 5A-B**). Similar PI(3,4,5)P3 binding inhibition of RAP1 was observed for 70 bp repeats (**Fig 5B**). Moreover, MST binding kinetics with 30 μM of PI(3,4,5)P3 increased rRAP1 Kd to telomeric and 70 bp repeats in ~6.5-fold and ~18.5-fold, respectively (**Fig 5C**, **Table 1**). Notably, PI(3,4,5)P3 did not affect rRAP1$^{301-560}$ or rRAP1$^{561-855}$ binding to telomeric or 70 bp repeats (Fig S6), implying that PI(3,4,5)P3 does not compete with Myb or MybL domains direct binding to DNA. PI(3,4,5)P3 inhibition of RAP1-DNA binding might be due to its association with RAP1 N-terminus causing conformational changes that affect Myb and MybL domains association with DNA.

Our data suggest a model in which PI(3,4,5)P3 levels control RAP1 binding to ESs and thus silencing and activation of VSG genes. To evaluate this model, we performed ChIP-seq with RAP1-HA in cells that exclusively express WT or Mut PIP5Pase. The Mut PIP5Pase expression results in local PI(3,4,5)P3 available for RAP1 binding (**Fig 4F**), whereas WT PIP5Pase dephosphorylates PI(3,4,5)P3 into PI(3,4)P2, which cannot bind RAP1 (24). The expression of Mut PIP5Pase abolished RAP1-HA binding to 70 bp, 50 bp, and telomeric repeats in all bloodstream and metacyclic ESs (**Fig 5D-G**). Notably, the decreased RAP1-HA binding to ESs correlates with increased expression of VSGs and ESAG genes (**Fig 5D-E**, RNAseq), indicating that PIP5Pase controls RAP1 binding to ESs and thus VSG gene expression. The increased level of VSG and ESAG mRNAs detected in cells expressing Mut PIP5Pase (**Fig 5D**) may reflect increased Pol I transcription. It is possible that the low levels of RAP1-HA at the 50 bp repeats affect Pol I accessibility to the BES promoter; alternatively, RAP1 association to telomeric or 70 bp repeats may affect chromatin compaction or folding impairing VSG and ESAG genes transcription. The expression of Mut PIP5Pase also removed RAP1-HA peaks in subtelomeric regions (**Fig 2F**), which might impact subtelomeric chromatin organization and thus VSG expression and recombination (**Fig 1D-F**). We showed that RAP1 interacts with PIP5Pase within a 0.9 MDa complex, and this association is stable in cells expressing the Mut PIP5Pase (24). Hence, RAP1 dissociation from ESs is unlikely the result of PIP5Pase mutations affecting the complex integrity. Our data indicate that PIP5Pase activity regulates RAP1 binding to DNA via PI(3,4,5)P3, thus controlling the reversible silencing of telomeric VSG genes.

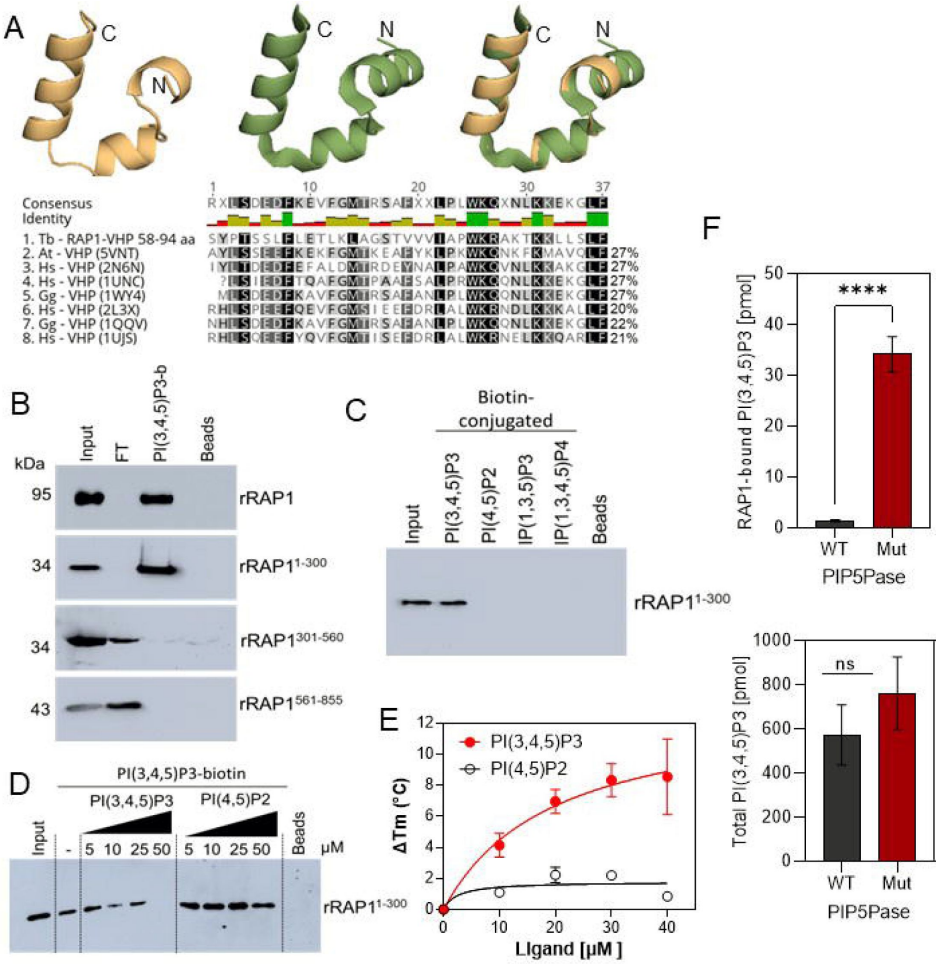

Fig 4.

rRAP1 binds to PI(3,4,5)P3 through its N-terminus.

A) Modeling and alignment of RAP1 VHP domain. *Left*, RAP1 modeled structure; *middle*, VHP domain structure of human supervillin protein (PDB accession number 2K6N); and *right*, superposition of *T. brucei* RAP1 modeled VHP and human supervilin VHP domains. Alignment of *T. brucei* RAP1 VHP with human (Hs), *Arabidopsis thaliana* (At), and *Gallus gallus* (Gg) VHP domains from Villin proteins. PDB accession numbers are indicated in parenthesis. % of aa identity to *T. brucei* sequence are shown. B) Binding assays with rRAP1, rRAP1$^{1-300}$, rRAP$^{301-560}$, or rRAP1$^{561-855}$ and PI(3,4,5)P3-biotin. Beads, Streptavidin-beads; FT, flow-through. Proteins were resolved in 10% SDS/PAGE and Western developed with α-His mAbs. C) Binding of His-tagged rRAP1$^{1-300}$ to biotinylated phosphoinositides or IPs. D) Binding of rRAP1$^{1-300}$ to PI(3,4,5)P3-biotin in presence of unlabelled PI(3,4,5)P3 or PI(4,5)P2. For C and D, proteins were analyzed as in B. E) Binding kinetics of rRAP1 with unlabelled PI(3,4,5)P3 or PI(4,5)P2. ΔTm, change in melting temperature. Data show the mean ± SDM of three biological replicates. F) Quantification of RAP1-bound PI(3,4,5)P3 (top) or total cellular PI(3,4,5)P3 (bottom) levels in *T. brucei* exclusively expressing WT or Mut PIP5Pase. Data show the mean ± SDM of four biological replicates. ****, *p*-value < 0.0001.

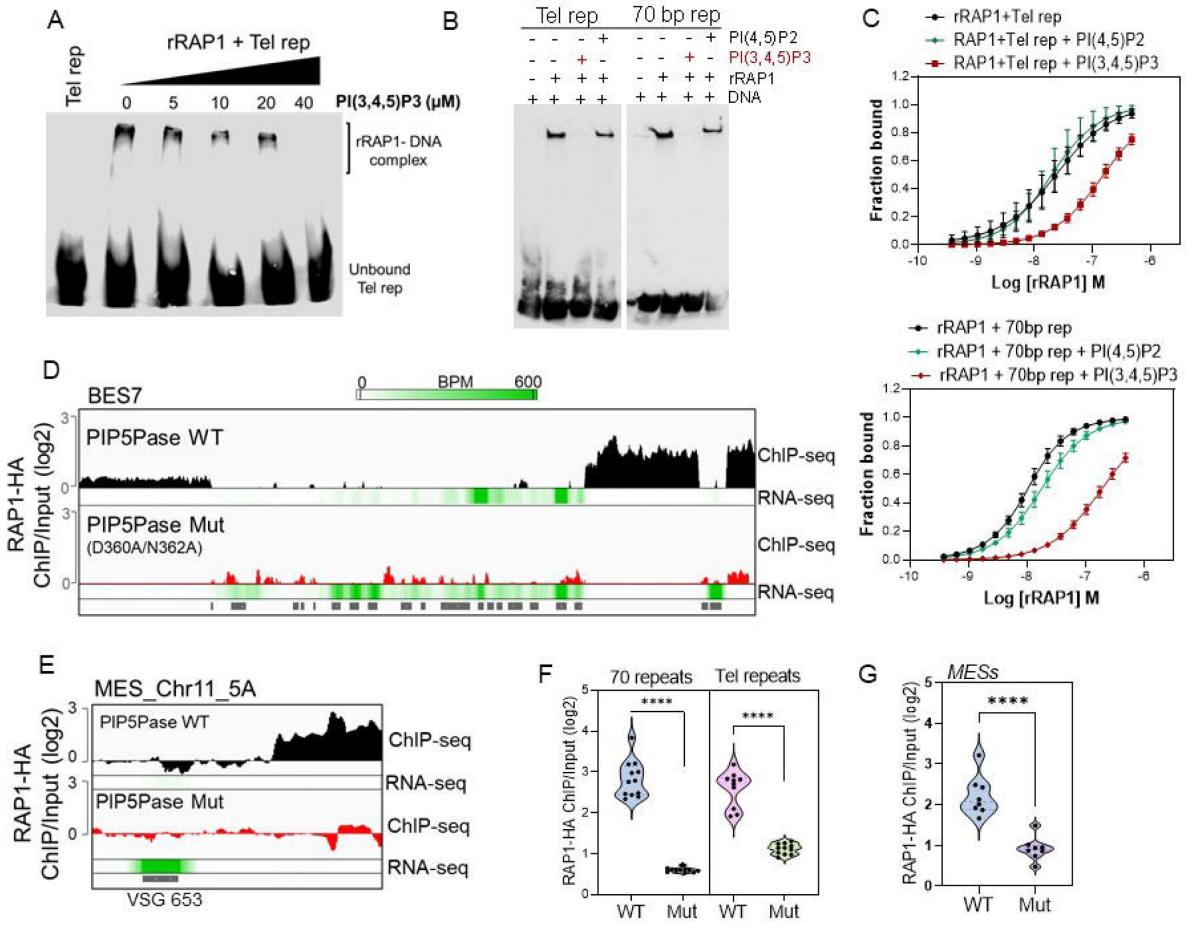

Fig 5.

PIP5Pase controls rRAP1 binding to telomeric ESs via PI(3,4,5)P3.

A) EMSA of rRAP1 with biotinylated telomeric repeats and increasing concentrations of PI(3,4,5)P3. B) EMSA of rRAP1 with biotinylated telomeric repeats (left) or 70 bp repeats (right) and 30 μM of PI(3,4,5)P3 or PI(4,5)P2. For A-B, samples were resolved in 6% native/PAGE, transferred to nylon membranes, and developed with streptavidin-HRP. C) MST binding kinetics of rRAP1 with Cy5-labelled telomeric repeats (top) or 70 bp repeats (bottom) with 30 μM of PI(3,4,5)P3 or PI(4,5)P2. Data show the mean ± SDM of four biological replicates. D-E) ChIP-seq of RAP1-HA binding to BES7 (D) or (MES_Chr11_5A) from cells that exclusively express WT or Mut PIP5Pase for 24h. RNA-seq comparing exclusive expression of Mut vs WT PIP5Pase for 24h is shown. F-G) Violin plots show RAP1-HA mean enrichment over 70 bp or telomeric repeats from all silent BESs (F) or MESs (G). Each dot represents an ES. BPM, bin per million. ChIP-seq and RNA-seq were performed in three biological replicates. ****, $p<0.0001$.

Discussion

We found that the reversible silencing of telomeric VSG genes in *T. brucei* is controlled by a phosphoinositide regulatory system. The system operates via PI(3,4,5)P3 regulation of RAP1-DNA binding and is controlled by PIP5Pase enzymatic activity. The system functions as an on/off genetic switch to control telomeric ES activation and silencing and indicates a mechanism to control the periodic switching of VSG genes during antigenic variation and VSG developmental silencing. The regulation requires PIP5Pase activity for continuous ES repression via dephosphorylation of PI(3,4,5)P3. PIP5Pase temporary inactivation results in the accumulation of PI(3,4,5)P3 bound to the RAP1 N-terminus. This binding displaces RAP1 Myb and MybL domains from DNA, likely due to RAP1 conformational changes, allowing polymerase elongation through the VSG gene. PI(3,4,5)P3 acts as a typical allosteric regulator controlling RAP1-DNA interactions and, thus, VSG transcriptional repression.

Our data indicate that regulation of PIP5Pase activity and PI(3,4,5)P3 levels play a role in VSG switching. Other phosphoinositide enzymes such as PIP5K or PLC, which act on PI(3,4,5)P3 precursors, also affect VSG expression and switching (23), arguing that this system is part of a cell-wide signaling network and includes the transcriptional and recombination machinery. The finding of RAP1 binding to subtelomeric regions other than ESs, including centromeres, requires further validation. Nevertheless, it suggests a role for RAP1 repressing subtelomeric chromatin. Chromatin conformational capture analysis showed that subtelomeric regions and centromeres (many subtelomeric in *T. brucei*) have a high frequency of interactions forming the boundaries of genome compartments in *T. brucei* (13). Disrupting PIP5Pase activity affects RAP1 association with those regions and, thus, might impact long-range chromatin interactions. This organization may explain RAP1's role in VSG recombinational switching (33) and the transcription of subtelomeric VSGs upon PIP5Pase mutation, RAP1 (29) or NUP1 knockdowns (34).

RAP1 and PIP5Pase interact and localize near the nuclear periphery (23, 24). RAP1 also associates with NUP1 (24), which knockdown derepresses silent VSG genes (34). PI(3,4,5)P3 and other phosphoinositides are synthesized in the endoplasmic reticulum (ER) and Golgi (35, 36) and distributed to organelles, including the nuclear membrane (23, 36). The scenario suggests a model in which RAP1 associates with silent telomeric ESs and lamina proteins at the nuclear periphery (13, 23, 34), where regulation of silencing and activation might occur. The compartmentalization of silent ESs near the nuclear lamina may prevent the association of factors required for ES transcription, including chromatin-associated proteins and RNA processing factors. In contrast, the active ES is depleted of RAP1, a process that might involve ES mRNAs competition for RAP1 binding to ES DNA (37), and it is enriched in proteins that facilitate transcription, including VEX2 and ESB1 (17, 38). Furthermore, the active ES localizes in a compartment that favours efficient processing of VSG mRNAs (39, 40). Hence, the active and silent ESs seem to occupy distinct subnuclear compartments and have specific associated proteins. Within this model, VSG switching may entail the inactivation of PIP5Pase, leading to reorganization of silent ES chromatin, e.g., RAP1 removal from ESs, ESs relocation away from the nuclear lamina, and perhaps changes in ES three-dimensional organization (Fig S8). Once RAP1 is dissociated from ESs, other factors, such as ESB1 and VEX2, may associate with the silent ESs to initiate transcription. Although the requirements for establishing VSG monogenic expression are unknown, it may entail the successful association of factors with ESs for their transcription or recruitment to the ESB (2, 39).

How the phosphoinositide signaling system is initiated to control VSG switching is unknown, but our data suggest an alternative non-stochastic model regulating antigenic variation. It is unknown if this signaling system regulates antigenic variation *in vivo*. Nevertheless, the data indicate that trypanosomes may have evolved a sophisticated mechanism to regulate antigenic variation that entails genetic and signaling processes, and such processes may be conserved in other pathogens that rely on antigenic variation for infection, e.g., *Plasmodium* and *Giardia*, broadening

opportunities for drug discovery. The allosteric regulation of RAP1 by PI(3,4,5)P3 denotes a mechanism for phosphoinositide regulation of telomere silencing. Given that telomere silencing is conserved and dependent on RAP1 in most eukaryotes, this regulatory system may be present in other eukaryotes.

Materials and Methods

Cell culture, cell lines, and growth curves

T. brucei bloodstream forms (BF) single marker 427 conditional null (CN) and V5- or HA-tagged cell lines were generated and maintained in HMI-9 at 37°C with 5% CO_2 as described (23). Cell lines that exclusively express wildtype (WT) or mutant D360A/N360A (Mut) PIP5Pase gene (Tb927.11.6270) were generated as previously described (24). The WT or Mut PIP5Pase mRNAs exclusively expressed from tubulin loci are 1.6 and 1.3-fold the WT PIP5Pase mRNA levels expressed from endogenous alleles in the single marker 427 strain. The fold-changes were calculated from RNA-seq counts per million from this work (WT and Mut PIP5Pase, Data S1) and our previous RNA-seq from single marker 427 strain (24). *T. brucei* 29.13 were maintained in SDM-79 medium supplemented with 10% FBS, G418 (2.5 µg/mL), and hygromycin (50 µg/mL) at 27°C. To generate *T. brucei* procyclic forms (PF) CN PIP5Pase, PF 29.13 was transfected with a V5-tagged PIP5Pase gene cloned into pLEW100-3V5 (23). The plasmid was integrated into the rRNA silent spacer, and transgenic cells were selected by resistance to phleomycin (5 µg/mL). The PIP5Pase endogenous alleles were then sequentially replaced by homologous recombination with PCR constructs containing about 500 bp of the PIP5Pase 5'UTR and 3'UTR flanking a puromycin or blasticidin drug resistance gene (23). The CRISPR/Cas9 ribonucleoprotein complex was used to cut the second endogenous allele and increase homologous recombination rates. Guides targeting 5' and 3' regions (see primer sequences in Table S2) of the PIP5Pase coding sequence were produced by in vitro transcription with T7 polymerase (Promega), and co-transfected with recombinant saCas9 Nuclease NLS Protein (Applied Biological Materials Inc.), and a PCR-based puromycin resistance construct containing 5'- and 3'-UTRs of the targeted gene. Note that this procedure increased the efficiency of recombination by about 20 times. Cumulative growth curves were performed by diluting *T. brucei* PFs to 2×10^6 parasites/mL in the absence or presence of tetracycline (tet, 0.5 µg/mL). The culture growth was counted every two days using a Coulter Counter (Beckman Coulter) for twelve days.

Immunofluorescence and Western blotting

Immunofluorescence: Immunofluorescence was done using *T. brucei* PF PIP5Pase CN, which expresses V5-tagged WT PIP5Pase in the presence of 0.1 µg/mL of tet. Mid-log growth phase parasites were washed three times in PBS with 6 mM glucose (PBS-G) for 10 minutes (min). Then, 2.0×10^6 cells were fixed in 2% paraformaldehyde in PBS for 10 min at room temperature (RT) onto poly L-lysine treated 12 mm glass coverslips (Fisher Scientific). The coverslips were washed three times in PBS, and cells permeabilized in 0.2% Nonidet P-40 in PBS for 10 min. Cells were washed five times in PBS, and then blocked for 1 hour (h) in 10% nonfat dry milk in PBS. After, cells were incubated in LJ-V5 mouse monoclonal antibodies (mAb) (Thermo Life Technologies) diluted 1:500 in 1% milk in PBS for 2 h at RT. The cells were washed five times in PBS and incubated in goat α-mouse IgG (H+L) Alexa Fluor (Invitrogen) 1:1,000 in 1% milk in PBS for 2 h at RT. Cells were washed five times in PBS and stained in 10 µg/mL of 4',6-diamidino-2-phenylindole (DAPI) diluted in PBS for 15 min at RT. Cells were washed four times in PBS, twice in water, and then mounted onto microscope glass slides (Fisher Scientific) using a mounting medium (Southern Biotech). Cells' images were acquired using a Nikon E800 Upright fluorescence microscope (Nikon). *Western blotting:* Western analyses were performed as previously described (25). Briefly, cleared lysates of *T. brucei* PFs were prepared in 1% Triton X-100 in PBS with 1X protease inhibitor cocktail (Bio-Vision) and mixed in 4X Laemmli buffer (Bio-Rad) with 710 mM β-mercaptoethanol and heated for 5 min at 95°C. Proteins were resolved in 10% SDS/PAGE and transferred to nitrocellulose

membranes (Sigma Aldrich). Membranes were probed for 2 h at RT (or overnight at 4°C) with mAb α-V5 (BioShop Canada Inc.) 1:2,500 in 6% milk in PBS 0.05% Tween (PBS-T). Membranes were incubated in 1:5,000 goat anti-mouse IgG (H+L)-HRP (Bio-Rad) in 6% milk in PBS-T, washed in PBS-T, and developed by chemiluminescence using Supersignal West Pico Chemiluminescent Substrate (Thermo scientific). Images were acquired on a ChemiDoc MP imaging system (Bio-Rad). Membranes were stripped in 125 mM glycine, pH 2.0, and 1% SDS for 30 min, washed in PBS-T, and re-probed with mAb anti-mitochondrial heat shock protein (HSP) 70 of *T. brucei* (gift from Ken Stuart, Center for Global Infectious Diseases Research, Seattle Children's) 1:25 in 3% milk in PBS-T, followed by 1:5,000 goat anti-mouse IgG (H+L)-HRP (Bio-Rad) in 3% milk in PBS-T and developed as described above.

Protein expression and purification

The *T. brucei* RAP1 (Tb927.11.370) recombinant protein was expressed and purified as described before (24). The RAP1 fragments rRAP1$^{1\text{-}300}$ (aa 1-300), rRAP1$^{301\text{-}560}$ (aa 301-560), or rRAP1$^{561\text{-}855}$ (aa 561-855) were amplified by PCR (see Table S2 for primers) from the *T. brucei* 427 genome and cloned into the pET-29a(+) vector (Novagen) using *NdeI* and *XhoI* restriction sites for the expression of proteins with a C-terminal 6xHis tag. Proteins were expressed and purified from 2 to 4 liters of *Escherichia coli* NiCo21(DE3) (New England Biolabs) as previously described (24). Briefly, lysates were sonicated in PBS supplemented with 5 mM dithiothreitol (DTT), 0.2 mg/mL lysozyme, 0.05% NP-40, 10% glycerol, and 1 mM PMSF. For rRAP1$^{1\text{-}300}$, this buffer was supplemented with 7 M of urea (Fisher Scientific). After sonication, His-tagged proteins in the cleared lysate were purified using Profinity™ IMAC Nickel Charged Resin (Bio-Rad) and eluted in 50 mM sodium phosphate buffer with 300 mM NaCl pH 8 and 300 mM imidazole (Fischer Scientific). Eluted proteins were dialyzed overnight at 4°C in binding buffer (25 mM HEPES, 150 mM NaCl, 10% glycerol, pH 7.5).

Phosphoinositide binding assays

Phosphoinositide binding assays were performed as previously described (20). Briefly, 1 µg of His-tagged recombinant protein (rRAP1, rRAP1$^{1\text{-}300}$, rRAP1$^{301\text{-}560}$, or rRAP1$^{561\text{-}855}$) was incubated with 1 µM of biotin-conjugated dioctanoylglycerol (diC8) PI(3,4,5)P3, diC8 PI(4,5)P2, InsP(1,4,5)P3 or InsP(1,3,4,5)P4 (Echelon Biosciences) rotating at RT for 1 h. Afterward, magnetic streptavidin beads (Sigma Aldrich) (previously blocked overnight at 4°C with 3% BSA in PBS) were added and incubated at 4°C for 1 h rotating. Using a magnetic stand, the mix was washed 5-6 times in 25 mM HEPES pH 7.5, 300 mM NaCl, 0.2% NP-40 and 0.1% Tween 20, and then eluted in 50 µL of 2x Laemmli buffer supplemented with 710 mM β-mercaptoethanol. Samples were boiled at 95°C for 5 min. Samples were resolved in 10% SDS-PAGE, transferred onto a nitrocellulose membrane (Sigma Aldrich), and probed with LJ-His mAb (Thermo Scientific) diluted 1:1,000 in 6% milk in PBS-T followed by α-mouse IgG HRP (Bio-Rad) diluted 1:5,000 in 6% milk in PBS-T. Membranes developed as indicated above.

Electrophoretic mobility shift assays

Synthetic single-stranded 5'-biotin-conjugated DNA sequences (Table S2) of telomeric repeats $(TTAGGG)_{10}$, 70 bp repeats (one repeat), and scrambled DNA (derived from telomeric repeats) were annealed (1:1 v/v, 10 µM) to reverse complementary unlabeled sequences (Table S2) (Integrated DNA Technologies) in a thermocycler by incubation at 95°C for 10 min, 94°C for 50 seconds, and a gradual decrease of 1°C every 50 seconds for 72 cycles in 200 mM Tris–HCl pH 7.4, 20 mM $MgCl_2$, 500 mM NaCl. 100 nM of annealed DNA were mixed with 1 µg of recombinant protein, and 2 mg/mL yeast tRNA (Life Technologies) in 20 mM HEPES, 40 mM KCl, 10 mM $MgCl_2$, 10 mM $CaCl_2$, and 0.2% N P-40, and incubated on a thermomixer (Eppendorf) at 37°C for 1 h. Then, 10 µL of the reaction was resolved on a 6% native gel (6% acrylamide in 200 mM Tris, 12,5 mM ethylenediaminetetraacetic acid (EDTA), pH 7.8 adjusted with acetic acid) at 100 V in 0.5 X TAE buffer (40 mM Tris, 20 mM acetic acid, and 1 mM EDTA). DNAs were transferred onto a nylon

membrane (Life Technologies) at 100 V for 30 min in 0.5x TAE. The membrane was blocked for 1 h at RT with nucleic acid detection blocking buffer (Life Technologies), then probed for 1 h at RT with streptavidin-HRP 1:5,000 (Genescript) diluted in PBS 3% BSA. The membrane was washed in PBS-T and developed using Supersignal West Pico Chemiluminescent Substrate (Thermo Fisher Scientific). Images were acquired with a ChemiDoc MP imaging system (Bio-Rad).

Microscale thermophoresis binding kinetics

Binding assays were performed using synthetic single-stranded 5'-Cy5 conjugated DNA sequences of telomeric repeats (TTAGGG)10, 70 bp repeats (one repeat), or scrambled DNA (derived from telomeric repeats) (see Table S2 for sequences). Sequences were annealed (1:1 v/v, 10 µM) to reverse complementary unlabeled sequences (Table S2, all sequences synthesized by Integrated DNA Technologies) in a thermocycler by incubation at 95°C for 10 min, 94°C for 50 seconds, and a gradual decrease of 1°C every 50 seconds for 72 cycles in 200 mM Tris–HCl pH 7.4, 20 mM $MgCl_2$, 500 mM NaCl. Then, 1 µM rRAP1 was diluted in 16 two-fold serial dilutions in 250 mM HEPES pH 7.4, 25 mM $MgCl_2$, 500 mM NaCl, and 0.25% (v/v) N P-40 and incubated with 20 nM telomeric or 70 bp repeats for 2 h at 37 °C, gently shaking. Afterward, samples were centrifuged at 2,000 x*g* for 5 min, loaded into Monolith™ capillary tubes (NanoTemper Technologies), and analyzed using the Monolith NT.115 MiscroScale Thermophoresis instrument with MO.Control software (NanoTemper Technologies). For binding assays in the presence of phosphatidylinositol phosphates (PIPs), the binding reaction was prepared as above but in the presence of 30 µM of diC8 PI(3,4,5)P3 or diC8 PI(4,5)P2. Four to six replicates were performed and presented as mean ± standard deviation. Data were analyzed using MO.Affinity Analysis (NanoTemper Technologies).

Differential Scanning Fluorimetry

T. brucei rRAP1 at 10 µM was incubated with 10 mM SYPRO Orange dye (ThermoFisher Scientific), filtered before use with a 0.22 µm sterile filter (Fisher scientific), in 15 mM HEPES, 150 mM NaCl, pH 7.0, and 10, 20, 30, or 40 µM of diC8 PI(3,4,5)P3, diC8 PI(4,5)P2, or no PIPs in 96-well microplates (Life Technologies). The plate was sealed with MicroAmp® Optical Adhesive Film (Life Technologies), and the reaction mixture was placed on ice for 1 h. Afterward, 20 µL of the reaction was added to a differential scanning fluorimetry plate (Life Technologies) and run using the Applied Biosystems StepOnePlus instrument (ThermoFisher Scientific) according to the manufacturer's instructions. Briefly, samples were run using continuous ramp mode with two thermal profiles: Step 1 at 25°C for 2 min and step 2 at 99°C for 2 min, with a ramp rate of 100% at step 1 and 1% at step 2. Experiments were performed in triplicate and presented as mean ± standard deviation. Data analysis was performed using the DSFworld (*https://gestwickilab.shinyapps.io/dsfworld/*) platform, and melting temperatures were calculated as the midpoint of the resulting fluorescence versus temperature curve.

RNA-seq and real-time PCR

Poly-A enriched RNAs were extracted from 1.0×10^8 *T. brucei* BFs CN PIP5Pase exclusively expressing V5-tagged PIP5Pase WT or mutant D360A/N362A for 24 h using the magnetic mRNA isolation kit (New England Biolabs) according to manufacturer's instructions. For procyclic forms, total RNAs were extracted from 5.0×10^8 *T. brucei* CN PIP5Pase growing in Tet + (0.5 µg/mL, no knockdown) or Tet – (knockdown) at 5h, 11h, 24h, 48h, and 72h using TRIzol (Thermo Fisher Scientific) according to manufacturer's instructions. The isolated mRNA samples were used to synthesize cDNA using ProtoScript II Reverse Transcriptase (New England Biolabs) according to the manufacturer's instructions. Real-time PCRs were performed using VSG primers as previously described (23). For RNA-seq, cDNA samples were purified using Totalpure NGS mag-bind (Omega-BioTek) at a 1.0x ratio (beads to cDNA volume). cDNA samples were eluted in 55 uL of water, then fragmented to a size range of 300bp – 1kb (average 700 bp) using an M220 Focused-ultrasonicator (Covaris) with 75 peak incidence power, 10% duty factor, and 200 cycles per burst for 35 seconds at 20 °C. The fragmented cDNAs were then used for RNA-seq library preparation for

Oxford nanopore sequencing (indicated below). Fifty fmol of barcoded libraries were sequenced in a MinION (Oxford Nanopore Technologies) using an FLO-MIN106 flow cell (Oxford Nanopore Technologies). Three biological replicates were performed.

ChIP-seq

ChIP-seq was performed with *T. brucei* BFs CN PIP5Pase expressing endogenously HA-tagged RAP1 and exclusively expressing V5-tagged PIP5Pase WT or mutant D360A/N362A. Cells were grown for 24h in the absence of tet, which results in the exclusive expression of WT or mutant PIP5Pase, in HMI-9 media supplemented with 10% FBS, 2 µg/mL of G418, 2.5 µg/mL of phleomycin, 0.1 µg/mL of puromycin, and 25 µg/mL of nourseothricin. A total of 3.0×10^8 cells at mid-log growth were fixed in 1% paraformaldehyde at 4°C for 10 min, then quenched for 10 min in 140 mM glycine. Fixed cells were spun down at 2000 x*g* for 10 min, washed twice in PBS, and processed for ChIP using truChIP Chromatin Shearing Kit with Formaldehyde (Covaris) according to the manufacturer's instructions. DNA was sheared to a size range of 0.5-1.5 kb (average 700 bp) using an M220 Focused-ultrasonicator (Covaris) with 75 peak incidence power, 5% duty factor, and 200 cycles per burst for 7 min at 7°C. ChIP was performed with a total of 15 µg of sonicated chromatin and 10 µg of Mab anti-V5 (BioShop Canada Inc.). The antibodies were cross-linked to Protein G Mag Sepharose Xtra (GE Healthcare) according to the manufacturer's instructions before immunoprecipitations. Antibody eluted chromatin was incubated with 20 units of Proteinase K (Thermo Fisher Scientific) and reverse cross-linked at 65°C overnight, followed by DNA extraction by phenol:chloroform:isoamyl alcohol (25:24:1, ThermoFisher Scientific) and isopropanol (v/v) precipitation. Samples were resuspended in water, and the DNA was selected for fragments above 300 bp using Totalpure NGS mag-bind (Omega-BioTek) at 0.85x ratio (beads to DNA volume). The DNA was eluted in water and used to prepare Oxford nanopore DNA sequencing libraries (indicated below). Fifty fmol of barcoded libraries was sequenced in a MinION (Oxford Nanopore Technologies) using an FLO-MIN106 flow cell (Oxford Nanopore Technologies). Three biological replicates were performed.

VSG-seq

T. brucei BFs PIP5Pase CN cell lines exclusively expressing V5-tagged PIP5Pase WT or mutant D360A/N362A were seeded at 1.0×10^3 parasites/mL in 50 mL of HMI-9 media supplemented with 10% FBS, 2 µg/mL of G418, 2.5 µg/mL of phleomycin, and grown for 24 h in the absence of tet, which results in the exclusive expression of WT or PIP5Pase mutant. Then, tet (0.5 µg/mL) was added to Mut PIP5Pase cells to rescue WT PIP5Pase expression, and cells were grown for an additional 60 h at 37°C and 5% CO_2 until they reached a concentration of 1.0×10^6 parasites/mL. RNA was then isolated using Trizol (Sigma-Aldrich) according to the manufacturer's instructions. cDNA was synthesized using random primers with 5x Protoscript II Reverse Transcriptase (New England BioLabs Ltd). cDNA was amplified using the VSG Splice Leader and SP6-VSG14mer primers (41) (Table S2) with denaturing at 94°C for 3 min, followed by 22 cycles of 94°C for 1 min, 42°C for 1 min, and 72°C for 2 min (41). Amplified fragments were purified using 0.55x beads/sample ratio with Mag-Bind® TotalPure NGS (Omega Bio-Tek). Amplicons were prepared for Oxford Nanopore sequencing using the ligation sequencing kit SQK-LSK110 (Oxford Nanopore Technologies) and PCR Barcoding Expansion kit (EXP-PBC001) according to the manufacturer's instructions (described below). Five fmol pooled barcoded libraries were sequenced in a MinION using a Flongle FLO-FLG001 flow cell (Oxford Nanopore Technologies). Experiments were performed in three biological replicates.

Clonal-VSG-seq

T. brucei BFs PIP5Pase CN cell lines seeded at 1.0×10^4 parasites/mL in 10 mL of HMI-9 media supplemented with 10% FBS and 2 µg/mL of G418 and 2.5 µg/mL of phleomycin in the absence of tet (tet -) for PIP5Pase knockdown, or in the presence of tet (tet +, 0.5 µg/mL) for PIP5Pase expression. After 24 h, tet (0.5 µg/mL) was added to the tet – cells to restore PIP5Pase expression

and cells were cloned by limited dilution. Briefly, the cells were diluted to a concentration of 1 parasite/300 µL and grown in 200 µL of media in 96-well culture plates (Thermo Scientific Inc.) and grown for 5-7 days at 37°C and 5% CO_2. Clones were collected from the plates and transferred to 24 well culture plates (Bio Basic Inc.) containing 2 mL of HMI-9 media with 10% FBS, 2 µg/mL of G418, 2.5 µg/mL of phleomycin, and 0.5 µg/mL of tet for 24 h to reach 1.0×10^6 parasites/mL. Afterward, cells were harvested by centrifugation at 2,000 x*g*, and pellets were collected for RNA extraction using the 96 Well Plate Bacterial Total RNA Miniprep Super Kit (Bio Basic Inc.) according to the manufacturer's instructions. cDNA was synthesized from extracted RNA samples using M-MuLV reverse transcriptase kit (New England Biolabs Ltd) based on the manufacturer's instructions and using customized primers splice leader (SL_F) and VSG barcoded primers (BCA_Rd_3'AllVSGs 1 to 96) (see Table S4 for primer sequences). The forward SL F primer is complementary to the splice leader sequence and has an Oxford nanopore barcode adapter sequence. The reverse primer contains a sequence complementary to the 3'-region conserved among VSG genes, a unique 6 random nucleotide barcode sequence, and an Oxford nanopore barcode adapter sequence for library preparation. The synthesized cDNAs were pooled in a 1.5 mL Eppendorf tube and amplified using the Oxford nanopore library barcoding primers (PCR Barcoding Expansion kit EXP-PBC001, Oxford Nanopore Technologies) with denaturing at 95° for 3 min, followed by 22 cycles of 95°C for 30 sec, 60°C for 30 sec, and 72°C for 2.30 min. Amplified fragments were purified using 0.55x beads/sample ratio NucleoMag® NGS magnetic beads (Takara Bio). Amplicons were prepared for Oxford Nanopore sequencing using the ligation sequencing kit SQK-LSK110 (Oxford Nanopore Technologies) according to the manufacturer's instructions (details described below). Five fmol of the barcoded library were sequenced in a MinION (Oxford Nanopore Technologies) using a Flongle FLO-FLG001 flow cell (Oxford Nanopore Technologies). A total of 118 and 94 clones of CN PIP5Pase cells tet + (PIP5Pase expression) and tet – (PIP5Pase knockdown), respectively, were analyzed.

Preparation of DNA libraries and Oxford nanopore sequencing

DNA libraries were prepared using the ligation sequencing kit SQK-LSK110 (Oxford Nanopore Technologies), according to the manufacturer's instructions. Briefly, the fragmented nucleic acids were end-repaired and A-tailed using the NEBNext Ultra II End Repair and A-Tailing Module (New England Biolabs). The samples were cleaned with Totalpure NGS mag-bind (Omega-BioTek) at 0.85x ratio (beads to DNA volume), then ligated with nanopore barcode adapters. The product was subsequently used for PCR amplification with barcoding primers (Oxford Nanopore Technologies). The PCR product was cleaned with Totalpure NGS mag-bind (Omega-BioTek) at a 0.85x ratio (beads to DNA volume) and ligated to motor proteins for DNA sequencing. The libraries were sequenced in a MinION Mk1C sequencer (Oxford Nanopore Technologies) using FLO-MIN106 flow cells (unless otherwise stated), and sequences were basecalled using the Guppy software (Oxford Nanopore Technologies). Sequencing information is available in Table S3 and fastq data is available in the Sequence Read Archive (SRA) with the BioProject identification PRJNA934938.

Computational analysis of RNA-seq, VSG-seq and ChIP-seq

RNA-seq or ChIP-seq fastq data from nanopore sequencing were mapped to *T. brucei* 427-2018 reference genome using minimap2 (*https://github.com/lh3/minimap2*) and the alignment data were processed with SAMtools (*https://github.com/samtools/samtools*). Reads with a nanopore sequencing Q-score > 7 were used for analysis, and the mean Q-score was 12. RNA-seq and VSG-seq (including clonal VSG-seq) mapped reads were quantified using featureCounts from package Subread (*https://bioconductor.org/packages/release/bioc/html/Rsubread.html*) and used for differential expression analysis using EgdeR (*https://bioconductor.org/packages/release/bioc/html/edgeR.html*). Alignments were filtered to remove supplementary alignments using samtools flags. Because RNA-seq reads were detected mapping to subtelomeric regions in cells expressing Mut PIP5Pase, differential expression analysis was also performed with alignments filtered for primary reads with a stringent mapping probability of 99,9% (mapQ 30) to eliminate potential multiple mapping reads. Read counts were obtained with featureCounts counting primary

alignments only and processed using EgdeR. For ChIP-seq, aligned reads mapped with minimap2 were processed with deepTools (*https://deeptools.readthedocs.io/en/develop/*) for coverage analysis using bamCoverage and enrichment analysis using bamCompare comparing RAP1-HA ChIP vs Input. Peak calling and statistical analysis were performed for broad peaks with Model-based Analysis of ChIP-Seq MACS3 (*https://github.com/macs3-project/MACS*), and data were visualized using the integrated genomics viewer tool (Broad Institute). To identify if RAP1-HA was mapping specifically to silent vs active ESs, mapped reads were filtered to remove supplementary and secondary alignments, i.e., only primary alignments were considered. Analyses were also performed with a minimum mapping probability of 90% and 99% (mapQ 10 and 20, see Fig S4). This stringent analysis removes reads aligning to multiple regions of the genome including reads mapping to multiple ESs, i.e., it retains reads aligning to specific regions of the ESs. Filtered reads were processed as described above using deepTools and MACS3 analysis. Scripts used for ChIP-seq, RNA-seq, and VSG-seq analysis are available at *https://github.com/cestari-lab/lab_scripts*. A specific pipeline was developed for clonal VSG-seq analysis, available at *https://github.com/cestari-lab/VSG-Bar-seq*.

Quantification of PI(3,4,5)P3

T. brucei BFs PIP5Pase CN cell lines exclusively expressing V5-tagged PIP5Pase WT or mutant D360A/N362A were grown in 100 mL HMI-9 media supplemented with 10% FBS, 2 µg/mL of G418, 2.5 µg/mL of phleomycin, and grown for 24 h in the absence of tet, which results in the exclusive expression of WT or Mut PIP5Pase. A total of 1.0×10^8 cells were used for PI(3,4,5)P3 quantification using Echelon's PIP3 Mass ELISA Kit (Echelon Biosciences), according to the manufacturer's instructions. Briefly, the cells were centrifuged at 2,000 x*g* at RT for 5 min, washed in PBS 6mM Glucose, and the supernatant was discarded. The cell pellets were resuspended in 10 mL of ice-cold 0.5 M Trichloroacetic Acid (TCA), incubated on ice for 5 min, then centrifuged at 1,000 x*g* for 7 min at 4°C. The supernatant was discarded, and the pellets were washed twice using 3 mL of 5% TCA/1 mM EDTA per wash at RT. Neutral lipids were extracted by adding 3 mL of MeOH: $CHCl_3$ (2:1) to the pellets and vortexed for 10 min at RT, followed by centrifugation at 1,000 x*g* for 5 min, and the supernatant discarded. This step was repeated once more to remove neutral lipids. 2.25 mL of MeOH:$CHCl_3$:HCl (80:40:1) was added to the pellets and vortexed for 25 min at RT, then centrifuged at 1,000 x*g* for 5 min to extract the acidic lipids. The supernatants were transferred to new 15 mL centrifuge tubes. 0.75 mL $CHCl_3$ and 1.35 mL 0.1 N HCl were added to the supernatants, vortexed for 30 seconds, then centrifuged at 1,000 x*g* for 5 min to separate the organic and aqueous phases. 1.5 mL of the organic (lower) phase was transferred to new 2 mL vials and vacuum dried using a SpeedVac (Thermo Scientific) at RT. The dried lipids were stored at -20°C until used. To quantify PI(3,4,5)P3 interacting with RAP1-HA, 300 mL of *T. brucei* BFs CN PIP5Pase expressing endogenously HA-tagged RAP1 and exclusively expressing V5-tagged PIP5Pase WT or mutant D360A/N362A were grown for 24h in absence of tet, which results in the exclusive expression of WT or mutant PIP5Pase, in HMI-9 media supplemented with 10% FBS, 2 µg/mL of G418, 2.5 µg/mL of phleomycin, 0.1 µg/mL of puromycin, and 25 µg/mL of nourseothricin. A total of 3×10^8 cells (PIP5Pase WT and Mut) were centrifuged at 2,000 x*g* at RT for 5 min, washed in 20 mL of PBS 6 mM glucose and then lysed in 5 mL of *T. brucei* cell lysis buffer (50 mM Tris, 150 mM NaCl, 2X protein inhibitor cocktail, 0.1% NP-40, and 1% Triton-X100), rotating at 4°C for 30 min. Lysates were centrifugated at 15,000 x*g*, 4°C for 30 min, and the cleared lysate was transferred to a new 15 mL falcon tube. 2% (100 µL) of the cleared lysate was collected for Western blot of HA-tagged RAP1 (input). The remaining cleared lysate was used for RAP1-HA immunoprecipitation with anti-HA monoclonal antibodies (ABClonal). 20 µg of anti-HA monoclonal antibodies crosslinked to protein G MicroBeads (GE Healthcare) were added to the cleared lysate and incubated overnight at 4 °C. Immunoprecipitated samples on beads were washed five times in wash buffer (50 mM Tris, 150 mM NaCl, 2X protein inhibitor cocktail, 0.1% NP-40). An aliquote corresponding to 20% of the beads-bound samples was collected and eluted in 6M Urea/100 mM Glycine pH 2.9 for Western blot analysis of immunoprecipitated RAP1-HA protein. The remaining samples on the beads (80%)

were used for acidic lipids extraction, as indicated above. The dried lipids were resuspended in PBS-T 0.25% Protein Stabilizer (PBS-T 0.25% PS), and PI(3,4,5)P3 content was measured using Echelon's PIP3 Mass ELISA Kit (Echelon Biosciences), according to the manufacturer's instructions.

Data presentation and statistical analysis

Data are shown as means ± SEM from at least three biological replicates. Comparisons among groups were made by a two-tailed t-test using GraphPad Prism. P-values < 0.05 with a confidence interval of 95% were considered statistically significant. Graphs were prepared using Prism (GraphPad Software, Inc.), MATLAB (Mathworks), or Integrated Genome Viewer (Broad Institute).

Abbreviations

- PI(3,4,5)P3
  phosphatidylinositol-(3,4,5)-triphosphate
- PIP5Pase
  phosphatidylinositol phosphate 5-phosphatase
- RAP1
  repressor activator protein 1
- ES
  expression site
- VSG
  variant surface glycoproteins.

Acknowledgements

This research was enabled in part by computational resources provided by Calcul Quebec (*https://www.calculquebec.ca/en/*) and the Digital Research Alliance of Canada (alliancecan.ca).

Funding

Canadian Institutes of Health Research grant CIHR PJT-175222 (IC)

The Natural Sciences and Engineering Research Council of Canada grant RGPIN-2019-05271 (IC)

Fonds de Recherche du Québec - Nature et technologie grant 2021-NC-288072 (IC)

Canada Foundation for Innovation grant JELF 258389 (IC)

McGill University fund 130251 (IC)

Islamic Development Bank Scholarship 600042744 (AOT)

FRQNT-Ukraine postdoctoral fellowship BUKX:2022-2023 337989 (OK)

The Natural Sciences and Engineering Research Council of Canada CGS M fellowship (ML)

Author contributions

Conceptualization: IC

Methodology: IC, AOT, TI, TS

Investigation: IC, AOT, RR, TI, ML, TS, OK

Visualization: IC, TS, AOT, ML

Funding acquisition: IC

Project administration: IC

Supervision: IC

Writing – original draft: IC

Writing – review & editing: IC, AOT, RR, TI, ML, TS, OK

Competing interests

Authors declare that they have no competing interests.

Data and materials availability

RNA-seq and ChIP-seq sequencing data is available in the Sequence Read Archive (SRA) with the BioProject identification PRJNA934938.

Supplementary Materials

Figs. S1 to S8

Tables S1 to S4

Data S1 to S2

References

1. Cestari I., Stuart K. (2018) **Transcriptional Regulation of Telomeric Expression Sites and Antigenic Variation in Trypanosomes** *Curr Genomics* **19**:119–132

2. Navarro M., Gull K. (2001) **A pol I transcriptional body associated with VSG mono-allelic expression in Trypanosoma brucei** *Nature* **414**:759–763

3. Horn D., Cross G. A. (1995) **A developmentally regulated position effect at a telomeric locus in Trypanosoma brucei** *Cell* **83**:555–561

4. Rudenko G., Blundell P. A., Dirks-Mulder A., Kieft R., Borst P. (1995) **A ribosomal DNA promoter replacing the promoter of a telomeric VSG gene expression site can be efficiently switched on and off in T. brucei** *Cell* **83**:547–553

5. Yang X., Figueiredo L. M., Espinal A., Okubo E., Li B. (2009) **RAP1 is essential for silencing telomeric variant surface glycoprotein genes in Trypanosoma brucei** *Cell* **137**:99–109

6. Baur J. A., Zou Y., Shay J. W., Wright W. E. (2001) **Telomere position effect in human cells** *Science* **292**:2075–2077

7. Myler L. R., et al. (2021) **The evolution of metazoan shelterin** *Genes Dev* **35**:1625–1641

8. Kyrion G., Liu K., Liu C., Lustig A. J. (1993) **RAP1 and telomere structure regulate telomere position effects in Saccharomyces cerevisiae** *Genes Dev* **7**:1146–1159

9. de Lange T. (2005) **Shelterin: the protein complex that shapes and safeguards human telomeres** *Genes Dev* **19**:2100–2110

10. Lototska L., et al. (2020) **Human RAP1 specifically protects telomeres of senescent cells from DNA damage** *EMBO Rep* **21**

11. Platt J. M., et al. (2013) **Rap1 relocalization contributes to the chromatin-mediated gene expression profile and pace of cell senescence** *Genes Dev* **27**:1406–1420

12. Figueiredo L. M., Cross G. A. (2010) **Nucleosomes are depleted at the VSG expression site transcribed by RNA polymerase I in African trypanosomes** *Eukaryot Cell* **9**:148–154

13. Muller L. S. M., et al. (2018) **Genome organization and DNA accessibility control antigenic variation in trypanosomes** *Nature* **563**:121–125

14. Figueiredo L. M., Janzen C. J., Cross G. A. (2008) **A histone methyltransferase modulates antigenic variation in African trypanosomes** *PLoS Biol* **6**

15. Schulz D., et al. (2015) **Bromodomain Proteins Contribute to Maintenance of Bloodstream Form Stage Identity in the African Trypanosome** *PLoS Biol* **13**

16. Glover L., Hutchinson S., Alsford S., Horn D. (2016) **VEX1 controls the allelic exclusion required for antigenic variation in trypanosomes** *Proc Natl Acad Sci U S A* **113**:7225–7230

17. Faria J., et al. (2019) **Monoallelic expression and epigenetic inheritance sustained by a Trypanosoma brucei variant surface glycoprotein exclusion complex** *Nat Commun* **10**

18. Deitsch K. W., Lukehart S. A., Stringer J. R. (2009) **Common strategies for antigenic variation by bacterial, fungal and protozoan pathogens** *Nat Rev Microbiol* **7**:493–503

19. Boothroyd C. E., et al. (2009) **A yeast-endonuclease-generated DNA break induces antigenic switching in Trypanosoma brucei** *Nature* **459**:278–281

20. Briggs E., Crouch K., Lemgruber L., Lapsley C., McCulloch R. (2018) **Ribonuclease H1-targeted R-loops in surface antigen gene expression sites can direct trypanosome immune evasion** *PLoS Genet* **14**

21. da Silva M. S., Hovel-Miner G. A., Briggs E. M., Elias M. C., McCulloch R. (2018) **Evaluation of mechanisms that may generate DNA lesions triggering antigenic variation in African trypanosomes** *PLoS Pathog* **14**

22. McCulloch R., Barry J. D. (1999) **A role for RAD51 and homologous recombination in Trypanosoma brucei antigenic variation** *Genes Dev* **13**:2875–2888

23. Cestari I., Stuart K. (2015) **Inositol phosphate pathway controls transcription of telomeric expression sites in trypanosomes** *Proc Natl Acad Sci U S A* **112**:E2803–2812

24. Cestari I., McLeland-Wieser H., Stuart K. (2019) **Nuclear Phosphatidylinositol 5-Phosphatase Is Essential for Allelic Exclusion of Variant Surface Glycoprotein Genes in Trypanosomes** *Mol Cell Biol* **39**

25. Cestari I. (2019) **Identification of Inositol Phosphate or Phosphoinositide Interacting Proteins by Affinity Chromatography Coupled to Western Blot or Mass Spectrometry** *J Vis Exp* **10**:3791–59865

26. Obado S. O., Bot C., Nilsson D., Andersson B., Kelly J. M. (2007) **Repetitive DNA is associated with centromeric domains in Trypanosoma brucei but not Trypanosoma cruzi** *Genome Biol* **8**

27. Akiyoshi B., Gull K. (2014) **Discovery of unconventional kinetochores in kinetoplastids** *Cell* **156**:1247–1258

28. Afrin M., Kishmiri H., Sandhu R., Rabbani M. A. G., Li B. (2020) **Trypanosoma brucei RAP1 Has Essential Functional Domains That Are Required for Different Protein Interactions. mSphere 5**

29. Afrin M., et al. (2020) **TbRAP1 has an unusual duplex DNA binding activity required for its telomere localization and VSG silencing** *Sci Adv* **6**

30. Kumar N., Zhao P., Tomar A., Galea C. A., Khurana S. (2004) **Association of villin with phosphatidylinositol 4,5-bisphosphate regulates the actin cytoskeleton** *J Biol Chem* **279**:3096–3110

31. Chiu T. K., et al. (2005) **High-resolution x-ray crystal structures of the villin headpiece subdomain, an ultrafast folding protein** *Proc Natl Acad Sci U S A* **102**:7517–7522

32. Meng J., McKnight C. J. (2009) **Heterogeneity and dynamics in villin headpiece crystal structures** *Acta Crystallogr D Biol Crystallogr* **65**:470–476

33. Nanavaty V., Sandhu R., Jehi S. E., Pandya U. M., Li B. (2017) **Trypanosoma brucei RAP1 maintains telomere and subtelomere integrity by suppressing TERRA and telomeric RNA:DNA hybrids** *Nucleic Acids Res* **45**:5785–5796

34. DuBois K. N., et al. (2012) **NUP-1 Is a large coiled-coil nucleoskeletal protein in trypanosomes with lamin-like functions** *PLoS Biol* **10**

35. Martin K. L., Smith T. K. (2006) **Phosphatidylinositol synthesis is essential in bloodstream form Trypanosoma brucei** *Biochem J* **396**:287–295

36. Kim Y. J., Guzman-Hernandez M. L., Balla T. (2011) **A highly dynamic ER-derived phosphatidylinositol-synthesizing organelle supplies phosphoinositides to cellular membranes** *Dev Cell* **21**:813–824

37. Gaurav A. K., et al. (2023) **The RRM-mediated RNA binding activity in T. brucei RAP1 is essential for VSG monoallelic expression** *Nat Commun* **14**

38. Lopez-Escobar L., et al. (2022) **Stage-specific transcription activator ESB1 regulates monoallelic antigen expression in Trypanosoma brucei** *Nat Microbiol* **7**:1280–1290

39. Faria J., et al. (2021) **Spatial integration of transcription and splicing in a dedicated compartment sustains monogenic antigen expression in African trypanosomes** *Nat Microbiol* **6**:289–300

40. Budzak J., Jones R., Tschudi C., Kolev N. G., Rudenko G. (2022) **An assembly of nuclear bodies associates with the active VSG expression site in African trypanosomes** *Nat Commun* **13**

41. Mugnier M. R., Cross G. A., Papavasiliou F. N. (2015) **The in vivo dynamics of antigenic variation in Trypanosoma brucei** *Science* **347**:1470–1473

Article and author information

Abdoulie O. Touray
Institute of Parasitology, McGill University, Sainte-Anne-de-Bellevue, QC H9X 3V9, Canada, Division of Experimental Medicine, Department of Medicine, McGill University, Montreal, QC, H4A 3J1, Canada

Rishi Rajesh
Institute of Parasitology, McGill University, Sainte-Anne-de-Bellevue, QC H9X 3V9, Canada

Tony Isebe
Institute of Parasitology, McGill University, Sainte-Anne-de-Bellevue, QC H9X 3V9, Canada

Tamara Sternlieb
Institute of Parasitology, McGill University, Sainte-Anne-de-Bellevue, QC H9X 3V9, Canada

Mira Loock
Institute of Parasitology, McGill University, Sainte-Anne-de-Bellevue, QC H9X 3V9, Canada

Oksana Kutova
Institute of Parasitology, McGill University, Sainte-Anne-de-Bellevue, QC H9X 3V9, Canada

Igor Cestari
Institute of Parasitology, McGill University, Sainte-Anne-de-Bellevue, QC H9X 3V9, Canada, Division of Experimental Medicine, Department of Medicine, McGill University, Montreal, QC, H4A 3J1, Canada
For correspondence: igor.cestari@mcgill.ca
ORCID iD: 0000-0003-3845-7535

Copyright

Editors

Reviewing Editor
Christine Clayton
Centre for Molecular Biology of Heidelberg University (ZMBH), retired, Heidelberg, Germany

Senior Editor
Dominique Soldati-Favre
University of Geneva, Geneva, Switzerland

Reviewer #1 (Public Review):

Comments on the original submission:

Trypanosoma brucei undergoes antigenic variation to evade the mammalian host's immune response. To achieve this, T. brucei regularly expresses different VSGs as its major surface antigen. VSG expression sites are exclusively subtelomeric, and VSG transcription by RNA polymerase I is strictly monoallelic. It has been shown that T. brucei RAP1, a telomeric protein, and the phosphoinositol pathway are essential for VSG monoallelic expression. In previous studies, Cestari et al. (ref. 24) has shown that PIP5pase interacts with RAP1 and that RAP1 binds PI(3,4,5)P3. RNAseq and ChIPseq analyses have been performed previously in PIP5pase conditional knockout cells, too (ref. 24). In the current study, Touray et al. did similar analyses except that catalytic dead PIP5pase mutant was used and the DNA and PI(3,4,5)P3 binding activities of RAP1 fragments were examined. Specifically, the authors examined the transcriptome profile and did RAP1 ChIPseq in PIP5pase catalytic dead mutant. The authors also expressed several C-terminal His6-tagged RAP1 recombinant proteins (full-length, aa1-300, aa301-560, and aa 561-855). These fragments' DNA binding activities were examined by EMSA analysis and their phosphoinositides binding activities were examined by affinity pulldown of biotin-conjugated phosphoinositides. As a result, the authors confirmed that VSG silencing (both BES-linked and MES-linked VSGs) depends on PIP5pase catalytic activity, but the overall knowledge improvement is incremental. The most convincing data come from the phosphoinositide binding assay as it clearly shows that N-terminus of RAP1 binds PI(3,4,5)P3 but not PI(4,5)P2, although this is only assayed in vitro, while the in vivo binding of full-length RAP1 to PI(3,4,5)P3 has been previously published by Cestari et al (ref. 24) already. Considering that many phosphoinositides exert their regulatory role by modulate the subcellular localization of their bound proteins, it is reasonable to hypothesize that binding to PI(3,4,5)P3 can remove RAP1 from the chromatin. However, no convincing data have been shown to support the author's hypothesis that this regulation is through an "allosteric switch".

Comments on revised manuscript:

In this revised manuscript, Touray et al. have responded to reviewers' comments with some revisions satisfactorily. However, the authors still haven't addressed some key scientific rigor issues, which are listed below:

1. It is critical to clearly state whether the observations are made for the endogenous WT protein or the tagged protein. It is good that the authors currently clearly indicate the results observed in vivo are for the RAP1-HA protein. However, this is not as clearly stated for in vitro EMSA analyses. In addition, in discussion, the authors simply assumed that the c-terminally tagged RAP1 behaves the same as WT RAP1 and all conclusions were made about WT RAP1.

There are two choices here. The authors can validate that RAP1-HA still retains RAP1's essential function as a sole allele in T. brucei cells (as was recommended previously). Indeed, HA-tagged RAP1 has been studied before, but it is the N-terminally HA-tagged RAP1 that has been shown to retain its essential functions. Adding the HA tag to the C-terminus of RAP1 may well cause certain defects to RAP1. For example, N-terminally HA-tagged TERT does not complement the telomere shortening phenotype in TERT null T. brucei cells, while C-terminally GFP-tagged TERT does, indicating that HA-TERT is not fully functional while TERT-GFP likely has its essential functions (Dreesen, RU thesis). Although RAP1-HA behaves similar to WT RAP1 in many ways, it is still not fully validated that this protein retains essential functions of RAP1. By the way, it has been published that cells lacking one allele of RAP1 behave as WT cells for cell growth and VSG silencing (Yang et al. 2009, Cell; Afrin et al. 2020, mSphere). In addition, although RAP1 may interact with TRF weakly, the interaction is direct, as shown in yeast 2-hybrid analysis in (Yang et al. 2009, Cell).

Alternatively, if the authors do not wish to validate the functionality of RAP1-HA, they need to add one paragraph at the beginning of the discussion to clearly state that RAP1-HA may not behave exactly as WT RAP1. This is important for readers to better interpret the results. In addition, the authors need to tune down the current conclusions dramatically, as all described observations are made on RAP1-HA but not the WT RAP1.

For a similar reason, the current EMSA results truly reflect how C-terminally His6-tagged RAP1 and RAP1 fragments behave. If the authors choose not to remove the His6 tag, it is essential that they use "RAP1-His6" to refer to these recombinant proteins. It is also essential for the authors to clearly state in the discussion that the tagged RAP1 fragments bind DNA, but the current data do not reveal whether WT RAP1 binds DNA. In addition, the authors incorrectly stated that "disruption of the MybL domain sequence did not eliminate RAP1-telomere binding in vivo" (lines 165-166). In ref 29, deletion of Myb domain did not abolish RAP1-telomere association. However, point mutations in MybL domain that abolish RAP1's DNA binding activities clearly disrupted RAP1's association with the telomere chromatin. Therefore, the current observation is not completely consistent with that published in ref 29.

2. There is no evidence, in vitro or in vivo, that binding PI(3,4,5)P3 to RAP1 causes conformational change in RAP1. The BRCT domain of RAP1 is known for its ability to homodimerize (Afrin et al. 2020, mSphere). It is therefore possible that binding of PI(3,4,5)P3 to RAP1 simply disrupts its homodimerization function. The authors clearly have extrapolated their conclusions based on available data. It is therefore important to revise the discussion and make appropriate statements.

- https://doi.org/10.7554/eLife.89331.2.sa1

Reviewer #2 (Public Review):

In this manuscript, Touray et al investigate the mechanisms by which PIP5Pase and RAP1 control VSG expression in T. brucei and demonstrate an important role for this enzyme in a signalling pathway that likely plays a role in antigenic variation in T. brucei. While these data do not definitively show a role for this pathway in antigenic variation, the data are critical for establishing this pathway as a potential way the parasite could control antigenic variation and thus represent a fundamental discovery.

The methods used in the study are generally well-controlled. The authors provide evidence that RAP1 binds to PI(3,4,5)P3 through its N-terminus and that this binding regulates RAP1 binding to VSG expression sites, which in turn regulates VSG silencing. Overall their results support the conclusions made in the manuscript. Readers should take into consideration that the epitope tags on RAP1 could alter its function, however.

There are a few small caveats that are worth noting. First, the analysis of VSG derepression and switching in Figure 1 relies on a genome which does not contain minichromosomal (MC) VSG sequences. This means that MC VSGs could theoretically be mis-assigned as coming from another genomic location in the absence of an MC reference. As the origin of the VSGs in these clones isn't a major point in the paper, I do not think this is a major concern, but I would not over-interpret the particular details of switching outcomes in these experiments.

Another aspect of this work that is perhaps important, but not discussed much by the authors, is the fact that signalling is extremely poorly understood in T. brucei. In Figure 1B, the RNA-seq data show many genes upregulated after expression of the Mut PIP5Pase (not just VSGs). The authors rightly avoid claiming that this pathway is exclusive to VSGs, but I wonder if these data could provide insight into the other biological processes that might be controlled by this signaling pathway in T. brucei.

Overall, this is an excellent study which represents an important step forward in understanding how antigenic variation is controlled in T. brucei. The possibility that this process could be controlled via a signalling pathway has been speculated for a long time, and this study provides the first mechanistic evidence for that possibility.

- https://doi.org/10.7554/eLife.89331.2.sa0

Author Response

The following is the authors' response to the original reviews.

> ***Reviewer #1 (Recommendations For The Authors):***
>
> 1. *The authors need to validate that RAP1-HA still retains its essential function. As indicated above, if RAP1-HA still retains its essential functions, cells carrying one RAP1-HA allele and one deleted allele are expected to grow the same as WT cells. These cells should also have the WT VSG expression pattern, and RAP1-HA should still interact with TRF.*

We demonstrated that C-terminally HA-tagged RAP1 co-localizes with telomeres by a combination of immunofluorescence and fluorescence in situ hybridization (Cestari and Stuart, 2015, PNAS), and co-immunoprecipitate telomeric and 70 bp repeats (Cestari et al. 2019 Mol Cell Biol). We also showed by immunoprecipitation and mass spectrometry that HA-tagged RAP1 interacts with nuclear and telomeric proteins, including PIP5Pase (Cestari et al. 2019). Others have also tagged T. brucei RAP1 with HA without disrupting its nuclear localization (Yang et al. 2009, Cell), all of which indicate that the HA-tag does not affect

protein function. As for the suggested experiment, there is no guarantee that cells lacking one allele of RAP1 will behave as wildtype, i.e., normal growth and repression of VSGs genes. Also, less than 90% of T. brucei TRF was reported to interact with RAP1 (Yang et al. 2009, Cell), which might be indirect via their binding to telomeric repeats rather than direct protein-protein interactions.

> *1. The authors need to remove the His6 tag from the recombinant RAP1 fragments before the EMSA analysis. This is essential to avoid any artifacts generated by the His6-tagged proteins.*

Our controls show that the His-tag is not interfering with RAP1-DNA binding. We show in Fig 3CG by EMSA and in Fig S5 by EMSA and microscale thermophoresis that His-tagged full-length rRAP1 does not bind to scrambled telomeric dsDNA sequences, which demonstrates that His-tagged rRAP1 does not bind unspecifically to DNA. Moreover, in Fig 3G and Fig S5, we show that His-tagged rRAP11-300 also does not bind to 70 bp or telomeric repeats. In contrast, the full-length His-tagged rRAP1, rRAP1301-560, or rRAP1561-855 bind to 70 bp or telomeric repeats (Fig 3C-G). Since all proteins were His-tagged, the His tag cannot be responsible for the DNA binding. We have worked with many different His-tagged proteins for nucleic acid binding and enzymatic assays without any interference from the tag (Cestari and Stuart, 2013; JBC; Cestari et al; 2013, Mol Cell Biol; Cestari and Stuart, 2015, PNAS; Cestari et al. 2016; Cell Chem Biol; Cestari et al. 2019 Mol Biol Cell).

> *1. More details need to be provided for ChIPseq and RNAseq analysis regarding the read numbers per sample, mapping quality, etc.*

Table S3 includes information on sequencing throughput and read length. Mapping quality was included in the Methods section “Computational analysis of RNA-seq and ChIP-seq”, starting at line 499. In summary, we filtered reads to keep primary alignment (eliminate supplementary and secondary alignments). We also analyzed ChIP-seq with MAPQ ≥20 (99% probability of correct alignment) to distinguish RAP1 binding to specific ESs, including silent vs active ES (ChIP-seq). We included Fig S4 to show the effect of filtering alignments on the active vs silent ESs. We used MAPQ ≥30 to analyze RNA-seq mapping to VSG genes, including those in subtelomeric regions. Our scripts are available at https://github.com/cestari-lab/lab_scripts. We also included in the Methods, lines 522-524: “Scripts used for ChIP-seq, RNA-seq, and VSG-seq analysis are available at https://github.com/cestari-lab/lab_scripts. A specific pipeline was developed for clonal VSG-seq analysis, available at https://github.com/cestarilab/VSG-Bar-seq.”

> *1. The authors should revise the Discussion section to clearly state the authors' speculations and their working models (the latter of which need solid supporting evidence). Specifically, statements in lines 218 - 219 and lines 224-226 need to be revised.*

The statement “likely due to RAP1 conformational changes” in line 228 discusses how binding of PI(3,4,5)3 could affect RAP1 Myb and MybL domains binding to DNA. We did not make a strong statement but discussed a possibility. We believe that it is beneficial to the reader to have the data discussed, and we do not feel this point is overly speculative. For lines 224-226 (now 234-235), the statement refers to the finding of RAP1 binding to centromeric regions by ChIP-seq, which is a new finding but not the focus of this work. To make it clear that it does not refer to telomeric ESs, we edited: “The finding of RAP1 binding to subtelomeric regions other than ESs, including centromeres, requires further validation.” Since RAP1 binding to centromeres is not the focus of the work, future studies are necessary to follow up, and we believe it is appropriate in the Discussion to be upfront and highlight this point to the readers.

Our model is based on the data presented here but also on scientific literature. We have reviewed the Discussion to prevent broad speculations. When discussing a model, we stated (line 245): “The scenario suggests a model in which …”, to state that this is a working model. Similarly, in Results (line 201) we included: “Our data suggest a model in which…”.

> *1. The authors should revise the title to reflect a more reasonable conclusion of the study.*

We agree that the title should be changed to imply a direct role of PI(3,4,5)P3 regulation of RAP1, which is not captured in the original title. This will provide more specific information to the readers, especially those broadly interested in telomeric gene regulation and RAP1. The new title is: PI(3,4,5)P3 allosteric regulation of repressor activator protein 1 controls antigenic variation in trypanosomes

> *1. The authors are recommended to provide an estimation of the expression level of the V5-tagged PIP5pase from the tubulin array in reference to the endogenous protein level.*

The relative mRNA levels of the exclusive expression of PIP5Pase mutant compared to the wildtype is available in the Data S1, RNA-seq. The Mut PIP5Pase allele’s relative expression level is 0.85fold to the WT allele (both from tubulin loci). We also showed by Western blot the WT and Mut PIP5Pase protein expression (Cestari et al. 2019, Mol Cell Biol). Concerning PIP5Pase endogenous alleles, we compared normalized RNA-seq counts per million from the conditional null PIP5Pase cells exclusively expressing WT or the Mut PIP5Pase alleles (Data S1, this work) to our previous RNA-seq of single-marker 427 strain (Cestari et al. 2019, Mol Cell Biol). We used the single-maker 427 because the conditional null cells were generated in this strain background. The PIP5Pase WT and Mut mRNAs expressed from tubulin loci are 1.6 and 1.3-fold the endogenous PIP5Pase levels in single-marker 427, respectively. We included a statement in the Methods, lines 275-278: “The WT or Mut PIP5Pase mRNAs exclusively expressed from tubulin loci are 1.6 and 1.3-fold the WT PIP5Pase mRNA levels expressed from endogenous alleles in the single marker 427 strain. The fold-changes were calculated from RNA-seq counts per million from this work (WT and Mut PIP5Pase, Data S1) and our previous RNA-seq from single marker 427 strain (24).”

> *1. The authors are recommended to provide more detailed EMSA conditions such as protein and substrate concentrations. Better quality EMSA gels are preferred.*

All concentrations were already provided in the Methods section. See line 356, in topic Electrophoretic mobility shift assays: “100 nM of annealed DNA were mixed with 1 µg of recombinant protein…”. For microscale thermophoresis, also see lines 375-376 in topic Microscale thermophoresis binding kinetics: “1 µM rRAP1 was diluted in 16 two-fold serial dilutions in 250 mM HEPES pH 7.4, 25 mM MgCl2, 500 mM NaCl, and 0.25% (v/v) N P-40 and incubated with 20 nM telomeric or 70 bp repeats…”. Note that two different biochemical approaches, EMSA and microscale thermophoresis, were used to assess rRAP1-His binding to DNA. Both show agreeable results (Fig 3 and 5, and Fig S5. Microscale thermophoresis shows the binding kinetics, data available in Table 1). The EMSA images clearly show the binding of RAP1 to 70 bp or telomeric repeats but not to scramble telomeric repeat DNA.

> ***Reviewer #2 (Recommendations For The Authors):***
>
> *Major comments:*
>
> *Figures*

> *All figures should have their axes properly labeled and units should be indicated. For many of the ChIPseq datasets it is not clear whether the authors show a fold enrichment or RPM and whether they used all reads or only uniquely mapping reads. Especially the latter is a very important piece of information when analyzing expression sites and should always be reported. The authors write, that all RNA-seq and ChIP-seq experiments were performed in triplicate. What is shown in the figures, one of the replicates? Or the average?*

ChIP-seq is shown as fold enrichment; we clarified this in the figures by including in the y-axis RAP1-HA ChIP/Input (log 2). We included in figure legends, see line 710: "Data show fold-change comparing ChIP vs Input.". For quantitative graphs (Fig 2B, D, and E, and Fig 5F and G), data are shown as the mean of biological replicates. Graphs generated in the integrated genome viewer (IGV, qualitative graphs) is a representative data (Fig 2A, C, and F, and Fig 5D-E). All statistical analyses were calculated from the three biological replicates. Uniquely mapped reads were used. We also included ChIP-seq analysis with MAPQ ≥10 and 20 (90% and 99% probability of correct alignment, respectively) to distinguish RAP1 binding to ESs. Fig S4 shows the various mapping stringency and demonstrates the enrichment of RAP1-HA to silent vs active ES.

> *Figure 1 is very important for the main argument of the manuscript, but very difficult (impossible for me) to fully understand. It would be great if the author could make an effort to clarify the figure and improve the labels. Panel Fig 1E. Here it is impossible to read the names of the genes that are activated and therefore it is impossible to verify the statements made about the activation of VSGs and the switching.*

We have edited Fig 1E to include the most abundant VSGs, which decreased the amount of information in the graph and increased the label font. We also re-labeled each VSG with chromosome or ES name and common VSG name when known (e.g., VSG2). We included Table S1 in the supplementary information with the data used to generate Fig 1E. In Table S1, the reader will be able to check the VSG gene IDs and evaluate the data in detail. We included in the legend, line 700: "See Table S1 for data and gene IDs of VSGs."

> *Figure 1F: This panel is important and should be shown in more detail as it distinguishes VSG switching from a general VSG de-repression phenotype. VSG-seq is performed in a clonal manner here after PIP5Pase KD and re-expression. To show that proper switching has occurred place in the different clones, instead of a persistent VSG de-repression, the expression level of more VSGs should be shown (e.g. as in panel E) to show that there is really only one VSG detected per clone. For example, it is not clear what the authors 'called' the dominant VSG gene.*

We showed in supplementary information Fig S1 B-C examples of reads mapping to the VSGs. Now we included a graph (Fig S1 D) that quantifies reads mapped to the VSG selected as expressed compared to other VSG genes considered not expressed). The data show an average of several clones analyzed. Other VSGs (not selected) are at the noise level (about 4 normalized counts) compared to >250 normalized counts to the selected as expressed VSGs.

> *As mentioned in the public comments, I don't see how the data from Fig 1E and 1F fit together. Based on Fig 1E VSG2 is the dominant VSG, based on Fig 1F VSG2 is almost never the dominant VSG, but the VSG from BES 12.*

In Fig 1E, the VSG2 predominates in cells expressing WT PIP5Pase, however, in cells expressing Mut PIP5Pase, this is not the case anymore. Many other VSGs are detected, and other VSG mRNAs are more abundant than VSG2 (see color intensity in the heat map). The

Mut cells may also have remaining VSG2 mRNAs (from before switching) rather than continuous VSG2 expression. This is the reason we performed the clonal analysis shown in Fig 1F, to be certain about the switching. While Fig 1F shows potential switchers in the population, Fig 1E confirms VSG switching in clones.

Many potential switchers were detected in the VSG-seq (Fig 1F, the whole cell population is over 107 parasites), but not all potential switchers were detected in the clonal analysis because we analyzed 212 clones total, a fraction of the over 107 cells analyzed by VSG-seq (Fig 1E). Also, it is possible that not all potential switchers are viable. A preference for switching to specific ESs has been observed in T. brucei (Morrison et al. 2005, Int J Parasitol; Cestari and Stuart, 2015, PNAS), which may explain several clones switching to BES12.

Note that in Fig 1F, tet + cells did not switch VSGs at all; all 118 clones expressed VSG2. We relabeled Fig 1F for clarity and included the VSG names. We added gene IDs in the Figure legends, see line 702 " BES1_VSG2 (Tb427_000016000), BES12_VSG (Tb427_000008000)…"

> *Statements in Introduction / Discussion*
>
> *The statement in lines 82/83 is very strong and gives the impression that the PIP5Pase-Rap1 circuit has been proven to regulate antigenic variation in the host. However, I don't think this is the case. The paper shows that the pathway can indeed turn expression sites on and off, but there is no evidence (yet) that this is what happens in the host and regulates antigenic variation during infection. The same goes for lines 214/215 in the discussion.*

We agree with the reviewer, and we edited these statements. The statement lines 82-83: "The data provide a molecular mechanism…" to "The data indicates a molecular mechanism…" For lines 224225: "and provides a mechanism to control…" to "and indicates a mechanism to control…". We also included in lines 261-262: "It is unknown if a signaling system regulates antigenic variation in vivo." Also edited lines 262-263: "…the data indicate that trypanosomes may have evolved a sophisticated mechanism to regulate antigenic variation...".

> *New vs old data*
>
> *In general, for Figures 1 - 4, it was a bit difficult to understand which panels showed new findings, and which panels confirmed previous findings (see below for specific examples). In the text and in the figure design, the new results should be clearly highlighted.*
> *Authors: All data presented is new, detailed below.*
>
> *Figure 1: A similar RNA-seq after PIP5Pase deletion was performed in citation 24. Perhaps the focus of this figure should be more on the (clone-specific) VSG-seq experiment after PIP5Pase re-introduction.*

This is the first time we show RNA-seq of T. brucei expressing catalytic inactive PIP5Pase, which establishes that the regulation of VSG expression and switching, and repression of subtelomeric regions, is dependent on PIP5Pase enzyme catalysis, i.e., PI(3,4,5)P3 dephosphorylation. Hence, the relevance and difference of the RNA-seq here vs the previous RNA-seq of PIP5Pase knockdown.

> *Figure 2: A similar ChIP-seq of RAP1 was performed in citation 24, with and without PIP5Pase deletion. Could new findings be highlighted more clearly?*

Our and others' previous work showed ChIP-qPCR, which analyses specific loci. Here we performed ChIP-seq, which shows genome-wide binding sites of RAP1, and new findings are shown here, including binding sites in the BES, MESs, and other genome loci such as centromeres. We also identified DNA sequence bias defining RAP1 binding sites (Fig 2A). We

also show by ChIP-seq how RAP1-binding to these loci changes upon expression of catalytic inactive PIP5Pase. To improve clarity in the manuscript, we edited lines 129-130: “We showed that RAP1 binds telomeric or 70 bp repeats (24), but it is unknown if it binds to other ES sequences or genomic loci.”

> *Figure 4: Binding of Rap1 to PI(3,4,5)P3, but not to other similar molecules, was previously shown in citation 24. Could new findings be highlighted more clearly?*

We published in reference 24 (Cestari et al. Mol Cell Biol) that RAP1-HA can bind agarose beadsconjugated synthetic PI(3,4,5)P3. Here, we were able to measure T. brucei endogenous PI(3,4,5)P3 associated with RAP1-HA (Fig 4F). Moreover, we showed that the endogenous RAP1-HA and PI(3,4,5)P3 binding is about 100-fold higher when PIP5Pase is catalytic inactive than WT PIP5Pase. The data establish that in vivo endogenous PI(3,4,5)P3 binds to RAP1-HA and how the binding changes in cells expressing mutant PIP5Pase; this data is new and relevant to our conclusions. To clarify, we edited the manuscript in lines 180-182: “To determine if RAP1 binds to PI(3,4,5)P3 in vivo, we in-situ HA-tagged RAP1 in cells that express the WT or Mut PIP5Pase and analyzed endogenous PI(3,4,5)P3 levels associated with immunoprecipitated RAP1-HA”.

> *Sequencing.*
> *I really appreciate the amount of detail the authors provide in the methods section. The authors do an excellent job of describing how different experiments were performed. However, it would be important that the authors also provide the basic statistics on the sequencing data. How many sequencing reads were generated per run (each replicate of the ChIP-seq and RNA-seq assays)? How long were the reads? How many reads could be aligned?*

The sequencing metrics for RNA-seq and ChIP-seq for all biological replicates were included in Table S3 (supplementary information). The details of the analysis and sequencing quality were described in the Methods section “Computational analysis of RNA-seq and ChIP-seq”. To be clearer about the analysis, we also included in Methods, lines 522-524: “Scripts used for ChIP-seq, RNA-seq, and VSG-seq analysis are available at https://github.com/cestari-lab/lab_scripts. A specific pipeline was developed for clonal VSG-seq analysis, available at https://github.com/cestari-lab/VSG-Bar-seq.”.

> *Minor comments:*
>
> *Figure 1B: I would recommend highlighting the non-ES VSGs and housekeeping genes with two more colors in the volcano plot, to show that it is mostly the antigen repertoire that is deregulated, and not the Pol II transcribed housekeeping genes. This is not entirely clear from the panel as it is right now.*

The suggestion was incorporated in Fig 1B. We color-coded the figure to include BES VSGs, MES VSGs, ESAGs, subtelomeric genes, core genes (typically Pol II and Pol III transcribed genes), and Unitig genes, those genes not assembled in the 427-2018 reference genome.

> *Were the reads in Figure 2a filtered in the same way as those in Figure 2C? To support the statements, only unique reads should be used.*

Yes, we also added Fig S4 to make more clear the comparison between read mapping to silent vs active ES.

> *It would be good if the authors could add a supplementary figure showing the RAP1 ChIP-seq (WT and cells lacking a functional PIP5Pase) for all silent expression sites.*

We had RAP1 ChIP-seq from cells expressing WT PIP5Pase already. We have it modified to include data from the Mutant PIP5Pase. See Fig S3 and S5.

> *In Figure 5D, after depletion of PIP5Pase, RAP1 binding appears to decrease across ESAGs, but ESAG expression appears to increase. How can this be explained with the model of RAP1 repressing transcription?*

We included in the Results, lines 208-212: “The increased level of VSG and ESAG mRNAs detected in cells expressing Mut PIP5Pase (Fig 5D) may reflect increased Pol I transcription. It is possible that the low levels of RAP1-HA at the 50 bp repeats affect Pol I accessibility to the BES promoter; alternatively, RAP1 association to telomeric or 70 bp repeats may affect chromatin compaction or folding impairing VSG and ESAG genes transcription.”.

> ***Reviewer #3 (Recommendations For The Authors):***
>
> *Line 114 - typo? Procyclic instead of procyclics:*

Fixed, thanks.

> *Line 233 - the phrasing here is confusing, may want to replace "whose" with "which" (if I am interpreting correctly):*

Thanks, no changes were needed. I have had the sentence reviewed by a Ph.D.-level scientific writer.

> *Methods - there is no description of VSG-seq analysis in the methods. Is it done the same way as the RNA-seq analysis? Is the code for analysis/generating figures available online?*

The procedure is similar. We included an explanation in Methods, lines 503-504: “RNA-seq and VSG-seq (including clonal VSG-seq) mapped reads were quantified…”. Also, in lines 522-54: “Scripts used for ChIP-seq, RNA-seq, and VSG-seq analysis are available at https://github.com/cestari-lab/lab_scripts. A specific pipeline was developed for clonal VSG-seq analysis, available at https://github.com/cestarilab/VSG-Bar-seq.”.

> *Fig 1H - Is this from RNA-seq or VSG-seq analysis of procyclics?*

The procyclic forms VSG expression analysis was done by real-time PCR. To clarify it, we included it in the legend “Expression analysis of ES VSG genes after knockdown of PIP5Pase in procyclic forms by real-time PCR”. We also amended the Methods, under the topic RNA-seq and real-time PCR, line 402-407: “For procyclic forms, total RNAs were extracted from 5.0x108 T. brucei CN PIP5Pase growing in Tet + (0.5 µg/mL, no knockdown) or Tet – (knockdown) at 5h, 11h, 24h, 48h, and 72h using TRIzol (Thermo Fisher Scientific) according to manufacturer's instructions. The isolated mRNA samples were used to synthesize cDNA using ProtoScript II Reverse Transcriptase (New England Biolabs) according to the manufacturer's instructions. Real-time PCRs were performed using VSG primers as previously described (23).”

> *Fig 2 A - Where it says "downstream VSG genes" I assume "downstream of VSG genes" is meant? the regions described in this figure might be more clearly laid out in the text or the legend*

Fixed, thanks. We included in the text in Results, line 140: “… and Ts and G/Ts rich sequences downstream of VSG genes”.

> *Fig 2E - what does "Flanking VSGs" mean in this context?*

We added to line 705, figure legends: “Flanking VSGs, DNA sequences upstream or downstream of VSG genes in MESs. “

> *Fig 2H - Why is the PIP5Pase Mutant excluded from the Chr_1 core visualization?*

We did not notice it. We included it now; thanks.